NTNU – Trondheim
Norwegian University of
Science and Technology

Resistance due to open moonpools on offshore ships

Eirik Nubdal Nesjø

MASTER THESIS IN MARINE TECHNOLOGY

SPRING 2015

FOR

Eirik Nesjø

Resistance due to open moonpools on offshore ships

Many types offshore vessels are equipped with moonpools, for deployment of ROVs and for lifting operations of different types. It is known that having the moonpools open during transit increases the resistance, but there is a lack of tools and detailed knowledge about the magnitude of resistance increase.

The objective of the master thesis is therefore to determine the added resistance of an open moonpool in calm water and in waves. The priority shall be on calm water. Furthermore, the priority should be to derive simple, general expressions rather than detailed calculations of a single case.

In the thesis the candidate shall present his personal contribution to the resolution of problem within the scope of the thesis work.

Theories and conclusions shall be based on mathematical derivations and/or logic reasoning identifying the various steps in the deduction.

The thesis work shall be based on the current state of knowledge in the field of study. The current state of knowledge shall be established through a thorough literature study, the results of this study shall be written into the thesis. The candidate should utilize the existing possibilities for obtaining relevant literature.

The thesis should be organized in a rational manner to give a clear exposition of results, assessments, and conclusions. The text should be brief and to the point, with a clear language. Telegraphic language should be avoided.

The thesis shall contain the following elements: A text defining the scope, preface, list of contents, summary, main body of thesis, conclusions with recommendations for further work, list of symbols and acronyms, reference and (optional) appendices. All figures, tables and equations shall be numerated.

The supervisor may require that the candidate, in an early stage of the work, present a written plan for the completion of the work. The plan should include a budget for the use of computer and laboratory resources that will be charged to the department. Overruns shall be reported to the supervisor.

The original contribution of the candidate and material taken from other sources shall be clearly defined. Work from other sources shall be properly referenced using an acknowledged referencing system.

The thesis shall be submitted electronically (pdf) in DAIM:
- Signed by the candidate

NTNU Trondheim
Norwegian University of Science and Technology
Department of Marine Technology

- The text defining the scope (signed by the supervisor) included
- Computer code, input files, videos and other electronic appendages can be uploaded in a zip-file in DAIM. Any electronic appendages shall be listed in the main thesis.

The candidate will receive a printed copy of the thesis.

Supervisor   : Professor Sverre Steen
Start   : 15.01.2015
Deadline   : 10.06.2015

Trondheim, 15.01.2015

Sverre Steen
Supervisor

Preface

This thesis has been written during the spring of 2015, as the finalising part of the Master of Technology education in Marin Technology at the Norwegian University of Science and Technology (NTNU) in Trondheim.

Several persons have guided my thought this work and deserves to be mentioned in gratitude.

I would like to thank my advisor Professor Sverre Steen at the Department of Marine Technology (NTNU) for his assistance. He has been orderly, interested and helpful along the process.

Several persons at MARINTEK needs to be recognised for their helpfulness and interesting conversations. Trygve Kristiansen and Kjetil Berget for their deep understanding of the topic. Last but not least Babak Ommani, whom without the simulation campaign would not have been possible.

Finally, I would like to extend my sincerest thanks to my fellow students throughout the years. André Risholm for the seed of ideas that lead to this topic and Jostein Opsahl, who wrote a related thesis during the same time, giving birth to many interesting discussions.

Trondheim, 10-06-2015

Eirik Nubdal Nesjø

Summary

A moonpool is a vertical well in a vessels hull that is exposed to the sea. Many types of offshore vessels are equipped with such a moonpool, to facilitate maritime operations. The water column inside of the moonpool is known to oscillate violently, and in model test, these oscillations have been connected to a resistance component. It is also well known that, during transit, an open moonpool will increase the resistance of the hull. Even so, most vessels are not equipped with any measures intended to reduce the added resistance from the moonpool.

This thesis has an objective aimed at building an understanding of the added resistance due to moonpool on offshore ships. The focus as been on forward velocities in calm waters, with an overall goal to derive general expressions describing the resistance.

After a thorough literature study, surprisingly few directly related experiments were found. It was established that the resistance consists primarily of the base resistance as the moonpool is a modification on the hull. Secondly it has been shown that the amplitude of the vertical piston-mode oscillation, is directly connected to a second resistance component. Expressions that estimates the amplitude development, and its connection to the resistance were found.

Numerical simulations were conducted using PVC3D, a software developed by MARINTEK. This solver is based on a hybrid method that combines the viscous flow with boundary conditions from potential flow theory.

The simulations were used to confirm the prediction models for the oscillation amplitudes. The oscillations are only observed within a smaller range of velocities. The expected range can be expressed by the normalised reduced velocity $U' = \frac{U}{\omega_0 l} \in [0.35 - 0.60]$ in calm waters.

In conclusion, it is expected that the total resistance of an offshore vessel increases in the area of 5-10 %, due to the existence of a moonpool. The piston-mode oscillation might contribute with an additional increase in the magnitude of 20-30 %. However, this is related to the maximum expected amplitude, which can be expected to be present in velocities well below the service speeds of offshore vessels. The resistance component related to the amplitude is related to a high level of uncertainties and should be a topic for further investigations.

Sammendrag

En moonpool er en vertikal brønn på et skrog som er eksponert mot sjøen i bunnen. Flere typer offshore skip har et slikt moonpool for å fasilitere maritime operasjoner. Det er et kjent fenomen at vannkolonnen som er inne i moonpoolen kan oscillere voldsomt. Det har i tidligere modellforsøk blitt bevist en motstandkomponent på skroget som er koblet med denne oscillasjonen. Det er en etablert sannhet at en åpen moonpool vil under transitt bidra til en tilleggs motstand på skroget. Til tross for dette, er det ikke vanlig å finne motstands begrensende installasjoner på moderne skrog.

Denne oppgaven har et overhengende mål for å bygge en bedre forståelse av tilleggs motstanden av en moonpool på offshore fartøy. Fokuset har vært rettet mot hastigheter i rolig sjø, og med et mål om å uttrykke denne motstanden med matematiske uttrykk.

Etter et gjennomgående litteratur studie, ble det funnet overraskende få direkte relaterte eksperimenter. Det ble etablert at motstanden kan deles opp i to ulike deler. Viktigst er den motstanden som kommer på grunn av moonpool som en endring på et skrog. Det ble også vist til at oscillasjonene kan gi opphav til en motstand som er lineær med amplituden inne i moonpoolen. Ulike uttrykk for å estimere amplitudeutviklingen og dens kobling med motstanden ble funnet.

Det ble gjort numeriske simulasjoner med PVC3D, en programvare utviklet hos MARINTEK. Denne løsningsmetoden baserer seg på en hybrid metode som kombinerer en ellers viskøs strømning, med grensebetingelser fra potensial teori.

Simulasjonen bekreftet utviklingen av oscillasjons amplituden for ulike hastigheter. Det ble vist at amplitudene kan forventes i et mindre hastighets intervall, uttrykt med den reduserte hastigheten $U' = \frac{U}{\omega_0 l} \in [0.35 - 0.60]$ i rolig sjø.

Med tanke på et offshore fartøy kan vi konkludere med at motstanden på grunn av moonpoolen, vil bestå av et konstant bidrag mellom 5 - 10 % og et variabelt bidrag på grunn av den vertikale oscillasjonen. Det siste bidraget kan vokse opp til 20 – 30 % i de mest ekstreme tilfeller. Dette siste bidraget er relatert til en stor usikkerhet og fortjener videre undersøkelser.

vi

Contents

I   Introduction   1

1   Introduction   3

2   Background Theory   9

II   Litterature Study   15

3   Published Experimental Results   17

List of Figures

List of Tables

List of Symbols

Symbol	Units	Description
x, y, z	m	Coordinate in the Cartesian Coordinate System
u, v, w	m/s	Velocities in the Cartesian Coordinate System
t	s	Time
a	m/s^2	Acceleration
m	kg	Mass
g	m/s^2	Gravitational Acceleration
F, f	N	Force
R	N	Resistance
P	N/m^2	Pressure
L	m	Length
B	m	Breadth
D	m	Draft of a hull
l	m	Length of moonpool
b	m	Breadth of moonpool
d	m	Draft of a moonpool
S	m^2	Cross-section area of moonpool
ρ	kg/m^3	Specific Density
ν	m^2/s	Kinematic Viscosity
C	–	Non-Dimensional coefficient
C_{MP}	–	Moonpool Resistance coefficient
C_{Base}	–	Base Drag coefficient
C_{FS}	–	Frictional coefficient
Re	–	Reynolds number
Fn	–	Froude number
St	–	Strouhal number
a_{ij}	–	Added mass coefficient
d'	–	Added draft coefficient
κ	–	Added draft parameter

b_{ij}^n	–	Damping coefficient
E_p	J	Potential Energy
E_k	J	Kinetic Energy
f	$1/s$	Frequecny
ω	rad/s	Radian frequency of a dynamic system
T	s	Period of a dynamic system
η	m	Position in a dynamic system
ζ	m	Wave elevation
h	m	Piston-mode elevation
h^*	m	Depth of domain
$\hat{h}$	m	Height of sloshing wave
U	m/s	Velocity of vessel
U'	m/s	Reduced velocity
U_∞	m/s	Free flow velocity
δ	m	Boundary layer thickness

Abbreviations

OSCV	Offshore Construction Support Vessel
CSV	Construction Support Vessel
IMR	Inspection, Maintenance and Repair
DVS	Diving Support Vessel
OCLV	Light Well Intervention
AHTS	Anchor Handling Tug Supply Vessels
PSV	Platform Supply Vessels
DP	Dynamic positioning
ROV	Remotely operated underwater vehicle
LOA	Length Over all
LPP	Length between perpendiculars
CFD	Computational fluid dynamics
CFL	Courant Fridrichs Lewy number
OpenFOAM	Open source Field Operation And Manipulation
PVC3D	Potential Visous Code 3D
RAM	Random Access Memory
CPU	Central Processor Unit

Part I

Introduction

Chapter 1

Introduction

1.1 Motivation

An increasing number of offshore vessels are equipped with a moonpool, either in direct connection with the vessels main purpose or indirectly as a contract speculation. In contrast to simple assumptions, there does not exist any closing mechanisms for the moonpool which can be considered mainstream. The vessels are normally delivered from the yard with a hatch that can be welded shut in the moonpool at keel-level, but this solution is seldom in use. Due to the installation complexity, the hatches are normally left ashore at the supply bases.

A moonpool is a great modification of the hull, and it is safe to assume that the modification increases the resistance of the hull. The magnitude of the connected fuel increase is an interesting question for all parties that are involved a vessel. However, it seems to be the industry standard and acceptance for that the moonpools remain open, even if it is seldom in use.

The following work seeks to build a deeper understanding of the dynamics of a moonpool. Quantify the added resistance of the hull, and to investigate if there exist some measures that can be taken in order to reduce the resistance.

The problem at hand was first mentioned in conversations with earlier fellow student André Risholm, that currently works at DOF Management AS.

1.2   Offshore Vessels and Moonpool

A range of vessels might have a moonpool to facilitate maritime operations. By moonpool, we refer to a vertical well in the hull that is exposed to the sea, as illustrated in figure 1.1. Such a moonpool can be found in a range of vessels from barges, drillships and offshore construction vessels. The focus of this study will be on the type of moonpool that are found on the latter type of vessels.
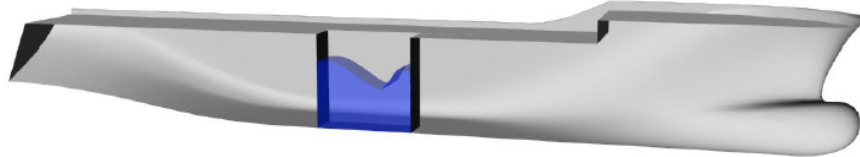
Figure 1.1: Illustration of a moonpool within an offshore vessel. (Hammargren and Törnblom (2012))

Offshore vessels can typically be divided into the follow group of vessels, based on their main capacities and operations conducted.

- Inspection, Maintenance and Repair (IMR)
- Diving Support Vessel (DVS)
- Light Well Intervention (LWI)
- Cable Laying Vessel (OCLV)
- Pipe laying
- Offshore Construction Support Vessel (OSCV or CSV)
- Anchor Handling Tug Supply Vessels (AHTS)

Common for most of these vessels are the use of highly advanced technologies, and the norm is that they are equipped with a moonpool, advance ROV's and a higher DP classification. For many of these vessel classifications, the moonpool is installed due to the nature of the vessels operational intentions. While for the latter type (AHTS), the moonpool can be installed as a speculation, giving the vessel access to a larger range of contracts.

The moonpool are designed to facilitate maritime operations, and by that we mean that they are utilised as a tool to achieve a greater operational window for their missions. Some of the arguments for the use of a moonpool are that the horizontal fluid motions inside the moonpool are small. The moonpool is often located close to the vessel's roll and pitch centre, thus reducing the vessels movement to its minimum. A moonpool creates opportunities for the instalment of special deployment systems that favours the moonpool over normal ship-side operations. As we explore more of our oil resources in Arctic conditions, the moonpool can also offer some shelter for the drifting ice.

1.3   Moonpool Geometry

The sketches in Figure 1.2 illustrates how a typical moonpool is designed on an offshore vessel. The moonpool has a cross-section at the opening denoted $S(-d)$ at the keel, as this area might be called the operational area of the moonpool.

(a) Adopted Berget et al. (2009)

(b) Adopted Spangeberg and Jacobsen (1983)
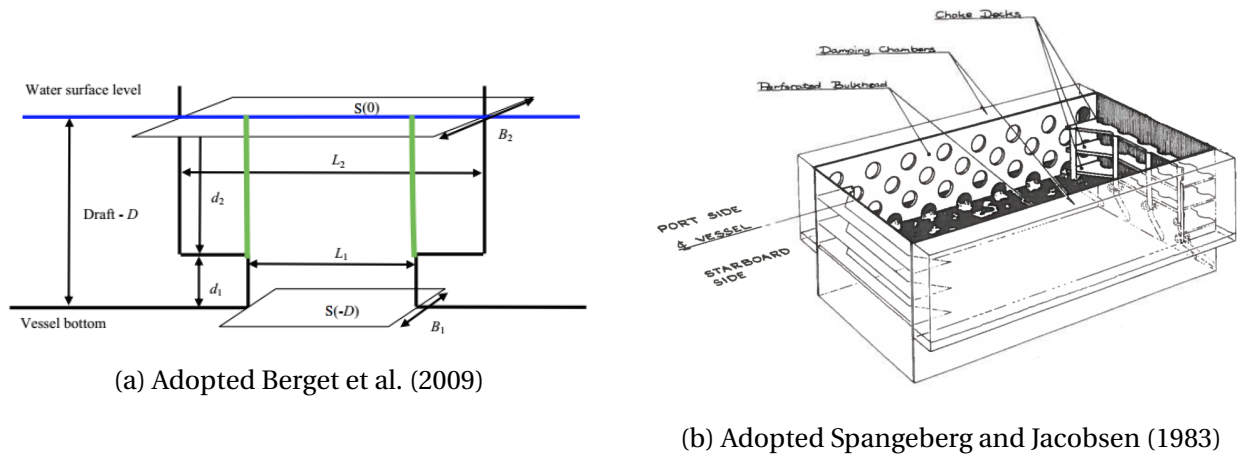
Figure 1.2: Illustration of typical moonpools with the design attributes.

The opening is kept constant for a distance d_1 before a sudden expansion of the cross-sectional area. This additional area is called a damping zone or cofferdam and reduces the vertical water motions.

Perforated bulkheads are simple walls with cut-outs, which are installed from the sharp edge of the area expansion and up through the free-water surface. These walls are installed to help the lowering of elements through the moonpool, and to reduce the horizontal water movements.

To add additional damping, it is expected to see choke decks installed inside of the inner wall. Simply put these are simple appendages or flanges that disrupt the flow.

1.4   Reported issues related to moonpool

The goal of the present work is to comment on the resistance on the hull due to the presence of the moonpool. There are also some other known issues that are related to the moonpools.

Operability

At the end of the day the moonpool is designed for a the vessel to perform a maritime operation; hence questions are raised for a definition of what waves and winds the operations can be conducted. The most critical factor is the vertical motions inside of the moonpool, causing a potential large load on any object that being launched through the water surface in the splash

zone. The term snatch loads are of critical evaluation, a slack in a hoist-wire that can lead to catastrophic failures.

As we move further north in our exploration of oil and gas, there follows a risk of ice. With the associated cold climate, problems related to the build-up of ice element in the moonpool arrises. Once an ice element is entrapped in a moonpool, it can be a demanding and time-consuming work to remove.

Green Water and Slamming

The vertical motions inside the moonpool can become very large and even exceed the freeboard. This will lead to green water inside of the hangar above the moonpool. This can both be a safety issue for the personal and the vessel and equipment. These oscillations will also cause slamming loads, that is loads that are typically concentrated on a limited are in a very short duration of time. These effects might lead the captain of the vessel to voluntary reducing the speed of the vessel or to change the heading. This will again lead to a loss of operability and lead to delays.

1.5   The Fleet of Vessels in the DOF Group

The problem at hand was inspired by ideas given during conversations with personnel from the DOF Group ASA. The company hold some of the largest fleet of offshore vessels in Norway, and it is convenient to present their fleet, to build a broader picture of the use of moonpool on offshore vessels.

As of 13th October 2014 (DOF Group ASA (2014)) the fleet consisted of 77 ships. The fleet is distributed as follows, 33 Construction Support Vessels (CSV), 20 Anchor Handling Tug Supply Vessels (AHTS) and 24 Platform Supply Vessels (PSV). And a new-build program consisting of 2 AHTS and 5 CVS pipe-layers.

The DOF fleet is recognised by their low age of the vessels, and the majority of the vessels have been designed and build of the company that today is VARD (previously STX and Aker Design). In Table A.1 the vessels with a work-class moonpool are listed. By the work-class definition, we have excluded the smaller ROV moonpool. As we can see that the typical moonpool has a square cross-section of 7,2 x 7,2 meters and that these vessels have a draft in the range of 6,3 to 8,5 meters, mean 7,4 meters.

1.6 Outline and Structure of Thesis

Part I gives a brief introduction to the motivations behind the problem and a brief theoretical background.

Part II is a literature study and is divided into three subchapters. The intention of the division is to separate the topics better, and to make the content more accessible for the reader. The basis for this part was made in the preparation project that was written in the autumn of 2014, but a lot of topics has been revisited and corrected.

Part III describes the simulations campaign that was undertaken. First an introduction chapter that explains some of the theoretical nature of the simulations and then a chapter that presents the numerical set-ups that were used. Lastly, the results are presented and discussed.

Part IV consists of the final conclutions and suggestions for further work.

Chapter 2

Background Theory

2.1   Introduction

In this chapter, we will present some background theory, to ease the explanations later in the report. It assumed that the reader has some insight in the fields of hydrodynamics and mechanics. A good overview of these topics can be found in the book Faltinsen (1993) *Sea Loads on Ships and Offshore Structures*, and in this report we seek to use the same notations in the formulations as Faltinsen.

2.2   Dimensional Analysis and Modelling

Model testing is done for practical reasons where one build a geometrical similar ship, but in a smaller scale. The scaling of resistance from model scale to full scale is done using non-dimensional resistance coefficients and the knowledge about the flow parameters. In the context of forces acting on a hull, the normal formulations for a coefficient is

$$C = \frac{R}{0.5 \rho S U^2} \tag{2.1}$$

Where ρ is the fluid density, U is the characteristic speed and S is the area of the wetted surface.

The most important dimensionless number in fluid dynamics is the Reynolds number, that qualitative expresses the ratio of inertial forces to viscous forces and is given by the following formula.

$$Re = \frac{UL}{v} \tag{2.2}$$

Where U is the characteristic speed, L is the characteristic length and v is the kinematic viscosity of the fluid. The Reynolds number describes the flow regime, and is used to determine if a flow is turbulent or laminar.

A ship model is in contact with the free-surface and the resistance contribution from the surface waves are of importance. These waves are gravity-driven, ands needs to be scaled as such. The Froude number expresses this ratio as following.

$$Fn = \frac{U}{\sqrt{gL}} \tag{2.3}$$

Where U is the characteristic speed, L is the characteristic length and g is gravitational acceleration (defined as $g = 9.81 \ m/s^2$).

2.3   Dynamic Systems

An oscillation is often exemplified with the periodic motion of a body or system of connected bodies displaced from a position of equilibrium.

(a) Simple damped body oscillator

(b) Histogram of a harmonic motion ($\zeta = 0$)

(c) Histogram of underdamped case ($\zeta < 1$)
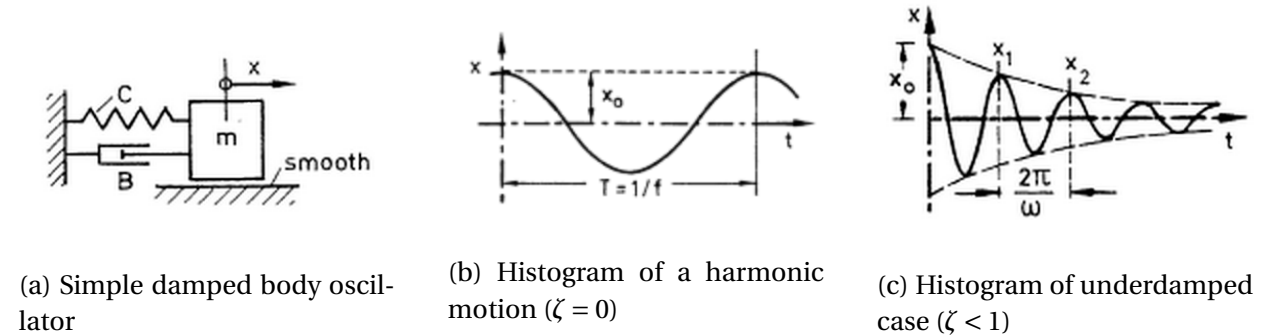
Figure 2.1: Illustration of a dynamic system and its resulting undamped and damped oscillation, adopted Naudascher and Rockwell (2012).

The simplest type of an oscillating motion is the undamped free vibration, represented by a mass-spring system. The mass m is exposed to an initial displacement x_0, and thus the stiffness C from the spring will set the mass to oscillate. Undamped means that there is no energy dissipating from the system, hence will this example result in an oscillation back-and-forth between two positions that is infinite in time. The equation of motion for such a system can be expressed by the following differential equations.

$$m\frac{d^2\eta}{dt^2} + C\eta = 0 \tag{2.4}$$

For which the simplest solution is $x(t) = x_0 sin(\omega t)$ and the undamped natural frequency ω_0 is expressed as

$$\omega_0 = \sqrt{\frac{C}{m}} \tag{2.5}$$

In most oscillations a third parameter called damping, B, plays a significant part. This is a resisting term of the oscillation that is proportional to the velocity, and are introduced on the left hand side of equation 2.4 as $B\frac{d\eta}{dt}$. This force is directly connected to the loss of energy in the system. A useful relation is the damping ratio

$$\zeta = \frac{B}{B_{crit}} = \frac{B}{2m\omega_0} = \frac{B}{2\sqrt{mC}} \tag{2.6}$$

The critical damping B_{crit} is defined such that motion is just brought to rest without overshooting the equilibrium position. This can also be expresses as the following

$$\zeta = \frac{1}{4\pi} \frac{\text{energy extracted per cycle of forced oscillation}}{\text{net energy participating in the cycle}} \tag{2.7}$$

2.3.1 Hydrodynamics Coefficients

As a body vibrates in an otherwise stagnant fluid, the fluid close to the body is set into motion so that the body becomes acted upon by a reaction force. The forced motions result in oscillating fluid pressure on the body surface. The resulting hydrodynamic forces directly coupled with the harmonic oscillation of the body, and are usually expressed as following.

$$F_k(t) = -A_{kj}\frac{d^2\eta}{dt^2} - B_{kj}\frac{d\eta}{dt} - C_{kj}\eta \tag{2.8}$$

Observe here that notation for the components subnotes kj, were k is the direction of the force due to a body movement in the j direction.

2.3.2 Uncoupled Single Body Model of Motions

The uncoupled model assumes that the vessel is restrained from movements, such only the water inside the moonpool is allowed to move. Due to the piston-like oscillations it is common to model the water-column as a solid body and restrict the movement to only vertical movement. We place the coordinate system in the areacenter of the moonpool, and define zero level at equilibrium which equals the outside water-level. Thus the equation of motion can be expressed as following.

$$(m + a_{33})\frac{d^2\eta}{dt^2} + b_{33}^1\frac{d\eta}{dt} + b_{33}^2\frac{d\eta}{dt}|\frac{d\eta}{dt}| + c_{33}\eta = F(t) \tag{2.9}$$

Here we have utilised the mass-spring model from Equation 2.4, and the hydrodynamic forces from Equation 2.8 has been added to the left hand side of the total equation. A quadratic damping term b_{33}^2 has been incorporated to obtain a satisfactory agreement with empirical results (see Aalbers (1984)).

Thus with the added mass included as a second contributor in the acceleration term, we need to included this added mass in the denominator of the undamped natural period (Eq. 2.10).

$$\omega_0 = \sqrt{\frac{c_{33}}{m + a_{33}}} \tag{2.10}$$

Then it is convenient to rewrite the latter equation in order to arrive to the expression for the natural period as it is expressed in the literature for moonpools. The stiffness for the moonpool comes from the free-surface and can be written as $c_{33} = \rho g S$ (see Faltinsen (1993)), where S is the cross-sectional area of the moonpool. The mass evaluated as equilibrium as $m = \rho d S$. Then for the added mass we utilise the convention of DNV (2011) and write $a_{33} = \rho \kappa S \sqrt{S}$.

$$\omega_0 = \sqrt{\frac{\rho g S}{\rho d S + \rho \kappa S \sqrt{S}}} = \sqrt{\frac{g}{d + d'}} \tag{2.11}$$

2.4   Flow Past Immersed Bodies

One important characteristic when a flow moves over a body, is that the is no slip. That means that the velocity on the body is zero. Thus it exists a boundary layer that is defined as the distance from the body where till the velocity is equal to $0.99 U_\infty$. The boundary layer thickness is highly dependent on the Reynolds number of the flow.

Flow separation means that the flow breaks away form the body. This occurs at a point along the body where the negative pressure gradient is strong and a consequence is that the wall shear stress changes sign and becomes negative in the direction of the flow. As the fluid separates from a body, it forms a separated region between the body and the main fluid stream. This region will have a back-flow due to the low pressure, and is hence recirculating.

2.4.1   Vortices

When the flow separates from a body there is normally a formation and shedding of circular fluid structures that are called vortices. This is often observed as a periodic phenomena and is referred to as vortex shedding. A important non-dimensional number for this phenomena is the Strouhal number, given as follows.

$$St = \frac{fL}{U} \tag{2.12}$$

Where f is the frequency of vortex shedding, U is the characteristic speed and L is the characteristic length. For a circular cylinder it is observed that the Strouhal number is keep nearly constant $St = 0.2$ for a large range for Reynolds numbers, from 10^2 to 10^5. The vortices might also originate due to a velocity discontinuity, as exemplified in Figure 2.2.
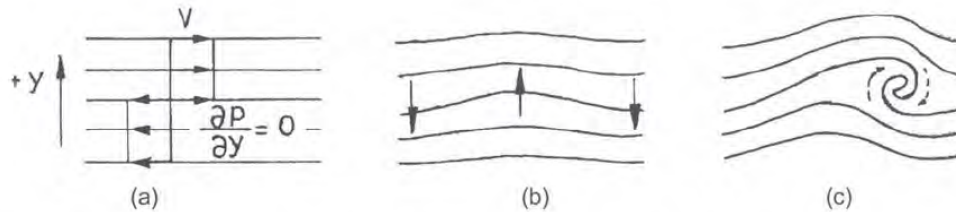
Figure 2.2: Vortex creation due to velocity discontinuity,Naudascher and Rockwell (2012).

2.4.2 Phase Lock-in and Hysteresis

Phase Lock-in and hysteresis are both phenomenas that are observed for some dynamic systems. Here we will exemplify these phenomena by the example of a circular body exposed to a normal flow, and shedding vortices.

Lock-in is when a system is being excited with an increasing frequency and the system response seems to lock into the natural frequency of the system. The phenomena is explained in Figure 2.3 where f_n if the natural frequency of the system, f_c is the frequency of the system response, marked as the solid line, and f_v is the frequency of excitation. For a circular cylinder, a constant St number will give a linear growth of the frequency of excitation as the velocity increases, see Equation 2.12. The units on the x-axis can be made non-dimensional with the reduced velocity ($U' = U/fl$) and the velocity at were the lock-in starts is referred to as the onset velocity.

Hysteresis is the name of a system where the dependence of the output is not only the input, but also its history of past inputs. In the context of a system with lock-in, this term is used to described that if the system is accelerated above the lock-in range, then the system can be decelerated without entering the lock-in at the same frequencies.
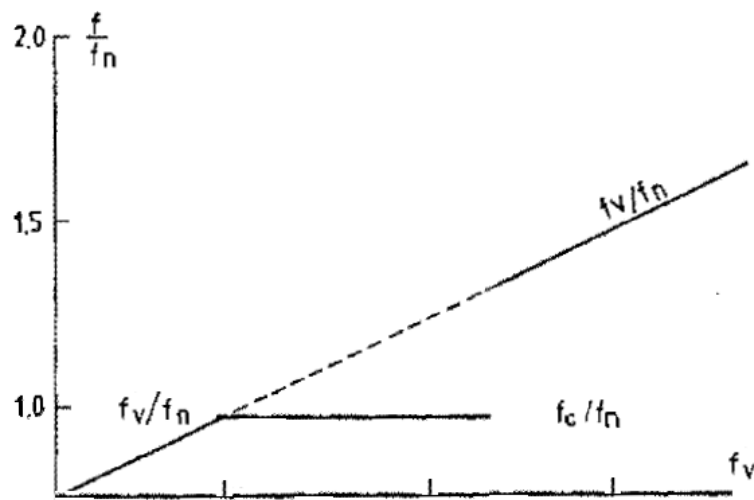
Figure 2.3: Example of the response frequency to a system with lock-in, adopted Faltinsen (1993).

Part II

Litterature Study

Chapter 3

Published Experimental Results

3.1 Introduction

In this chapter, we will present a summary of the existing experimental results. That is, experiments that are directly related to the water oscillation of a moonpool in a moving body, and how these oscillations relate to the resistance of the body. The results of the experiments will be presented in a logical order and commented upon. This is to build a build a basic understanding of the phenomena before we move on to establish mathematical formulations.

Most of the figures are taken directly from the papers and some do include prediction models or linear fittings. The details of these will be presented in the later chapters.

3.2 Descriptions of Experiments

English (1976) published what seems to be the first paper to investigate the water motions inside of the moonpool and the potential connection to the resistance of the hull. In this work, a model of unknown size is towed with a square moonpool, up to velocities of $Fn = 0.25$. English focused on the water motions and how to potentially reduce them by altering the geometry of the moonpool opening.

Fukuda (1977) published the year later a paper that goes more in depth into the exact problem of moonpool oscillations and resistance. He performed a range of experiments utilising four different models with both rectangular and circular moonpools. The models were between 2 and 4 meters long and was towed in velocities up to $Fn = 0.16$. It needs to be pointed out that this paper does only exist in Japanese, but the figures and their accompanying text is in English.

Cotteleer (2000) investigated the water motions and resistance in the moonpool of a drillship, caused by forward ship speed. The model was 4.2 meters long and fitted with a square moonpool that measured 0,256 meters in length and breath. The draft was altered to investigate

the dependence of this variable. The towing speed went up to $Fn = 0.265$.

van 't Veer and Tholen (2008) builds further on the model test campaign of Cotteleer with a reconstruction of the same model. As an extension to the work of Cotteleer, the focus in this work was influence of the length of the moonpool. The speeds were tested up to $Fn = 0.210$.

Kristiansen (2006) investigated the resistance influence of the moonpool on a model of a light construction vessel. The experiments were run at high velocities and several reduction alternatives were tested. In Froude numbers the velocity range were 0.19 to 0.28, and no piston-mode oscillation was observed.

Fukuda and Yoshii (2009) investigated the possibility to replicate the results from Fukuda (1977) original paper with a two-dimensional numerical model.

3.3   Dominating Oscillation Mode

The water inside of a moonpool is free to oscillate in two different oscillatory motions, the vertical piston-mode and the horizontal sloshing-mode. These two modes can also occur simultaneously, but it is normal to differentiate based on the dominating oscillation mode.

The horizontal sloshing-mode is a common phenomena for fluids in a closed container, and is commonly described as a standing wave within a closed confinement. The vertical piston-mode is a rather special phenomena, but is shared with other semi-entrained vertical gaps. Or in simpler words, vertical gaps were the water is confined and exposed to the free-surface. The name and reference to a piston comes from that fact that the water inside of the water column seems to have a uniform movement.
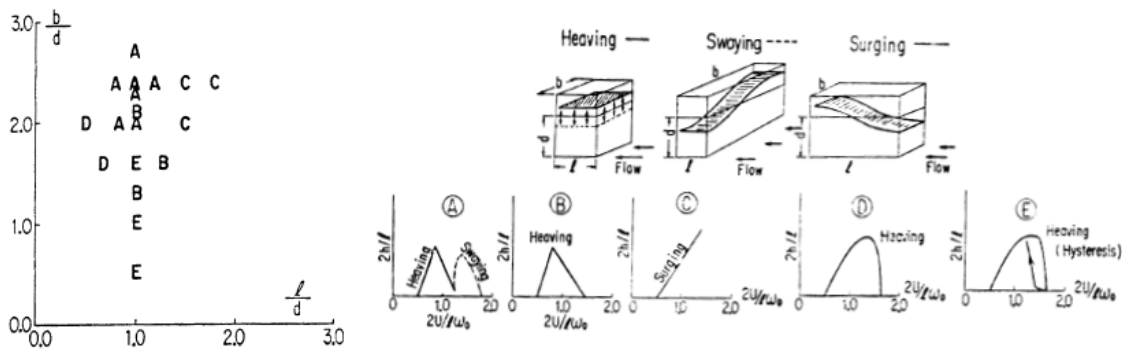
Figure 3.1: Description of the dominating oscillation in a rectangular moonpool, adopted Fukuda (1977).

As long as the vessel has a forward speed or a current is passing under a moonpool, one might expect some form of sloshing to be present. In the right conditions, the piston-mode will become the dominating form of water movement. Fukuda (1977) shows rather simply how these two modes are dependent on the geometry of the moonpool and the velocity of the vessel.

In Figure 3.1 we see on the left hand side which behaviour that is observed for different geometrical configurations. The behaviours are categorised into five distinct different cases (A-E), that develops depending on the vessel speed. The different cases are illustrated at the right hand side, and the velocity expressed as two times the reduced velocity. h is these graphs the amplitude of the oscillation. Thus $2h/d$ is the ratio between the height of the oscillation and the draft of the moonpool.

Offshore vessels are mostly equipped with moonpools that have a square cross-section and with a breath to draft ration less than unity. From figure 3.1 we can thus expect a oscillates that behaves like the category E. Observe that for longer moonpool the sloshing behaviour becomes dominant, and for shallower moonpools the shape of the expected amplitudes changes.

3.4 Oscillation Frequencies

3.4.1 Natural Frequency

Picking up the formulations for the natural frequency as given in Equation 2.11 by DNV, ($\omega_0 = \sqrt{\frac{g}{d+\kappa\sqrt{S}}}$), we see that an important part of the equation was not formulated to its full extent. The added draft for the oscillating water column is a hot topic that will be discussed in later sections. One simple way to estimate the value of κ is however to perform tests on a range of geometries and seek a linear connection between the results. In Figure 3.2 we see a example of this method.
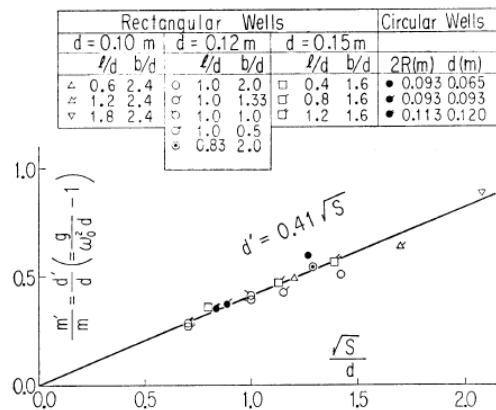
Figure 3.2: Natural frequency of the piston-mode for some moonpool geometries, Fukuda (1977).

3.4.2   Frequency of Oscillation

Based on the findings of an hysteresis behaviour as in motion that is denoted E in Figure 3.1, it is of interest investigate the observed frequency of oscillation.
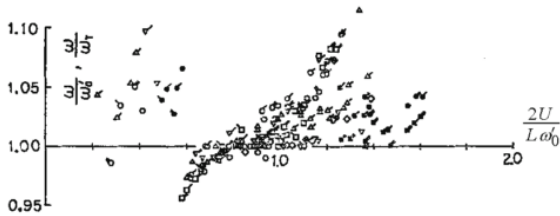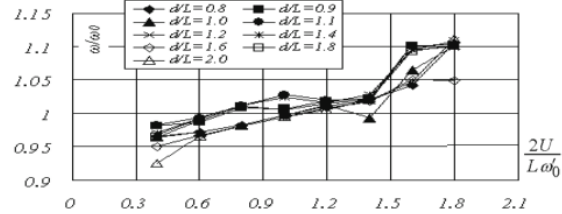
(a) Fukuda (1977)   (b) Fukuda and Yoshii (2009)

Figure 3.3: Frequency of moonpool oscillations with increasing velocity

As we can see from Fukuda's first paper there seem to a lock-in effect on the observed frequency. This results can be explained by phase lock-in as discussed in Section 2.4.2. The numerical results from Fukuda and Yoshii shows an agreement to the same phenomenon, even in only two dimensions.

3.5   Oscillation Amplitude
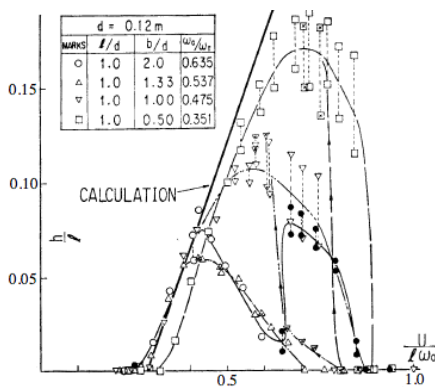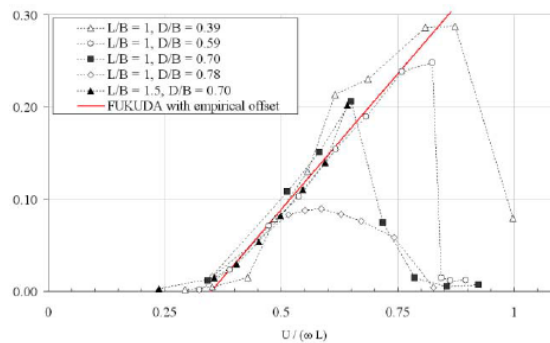
(a) Fukuda (1977)   (b) van 't Veer and Tholen (2008)

Figure 3.4: Amplitude of vertical oscillation as function of the reduced velocity.

In Figure 3.4 we see that the non-dimensional amplitude is a linear function of the reduced velocity, until a peak amplitude and a rapid and possibly a nonlinear decrease. The amplitude is made non-dimensional with regards of the length of the moonpool in occurrence of the use of the same length in the expression for the reduced velocity.

3.6 Resistance

3.6.1 Base Resistance

Kristiansen (2006) conducted a towing test on a model of the IMR vessel that today bears the name Edda Fauna. This is a ship that is 109 meters long and it is based on the ST-225 design from Skipsteknisk, (DeepOcean (2008)). As already mentioned the velocities where so high that no considering oscillation was observed. Scaled up to full-scale velocities the towing test were run at 12-18 knots, and the reported increase in resistance was 5,8-6,2 %.

3.6.2 Resistance due to oscillations

Already in the works of English (1976) it is observed and discussed that the variation of the resistance of the vessel, due to the moonpool, is in phase with the water column oscillations. In the Figures 6.4 and 6.4 we see the plots from the early experiments from English and Fukuda. In both figures the authors have included a prediction based linear momentum that will be explained in details later in the text.
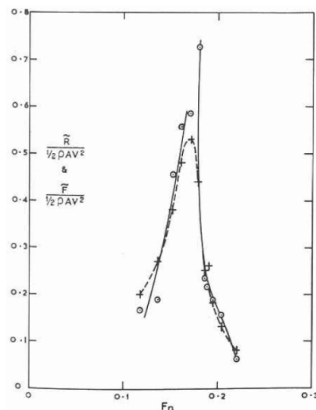
(a) English (1976)
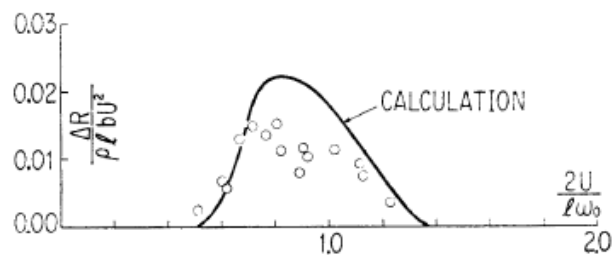
(b) Fukuda (1977)

Figure 3.5: Moonpool resistance coefficient as a function of a non-dimensional velocity.

The newer experiments of Cotteleer (2000) and van 't Veer and Tholen (2008) connects the resulting resistance with the amplitude of the oscillations. Which is a natural step, since we can decompose the problem into first estimate the amplitude and then the resistance. In many design problems the amplitude alone is a important parameter. The results that are given in Figures 3.6a and 3.6b shows for a potential linear connection. These two figures includes the base resistance as the constant term in the linear prediction.
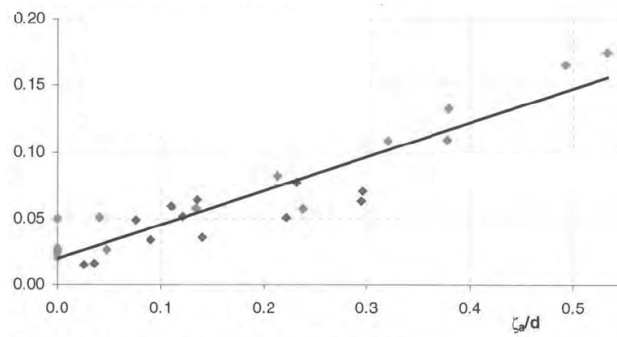
(a) Cotteleer (2000)
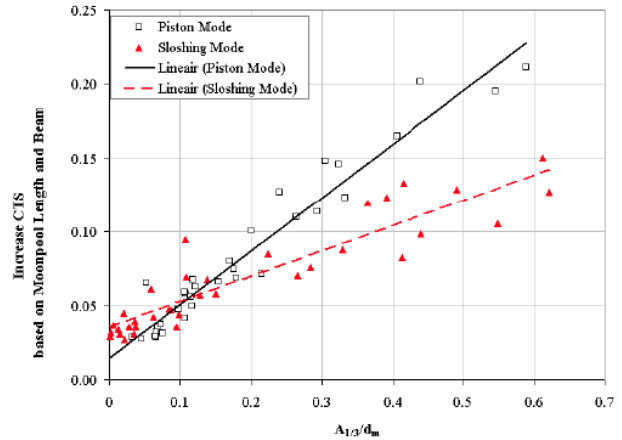
(b) van 't Veer and Tholen (2008)

Figure 3.6: Moonpool resistance coefficient as a function of non-dimensional amplitude.

In the work of van 't Veer and Tholen (2008) they comment that the overall resistance for a vessel with a square moonpool, increased a total of 60 % for the most extreme condition. It is assumed that this number is the comparison of a closed hull and a moonpool with maximum piston-mode amplitude. For longer moonpools, they observed even higher resistances. The constant resistance from the open moonpool without oscillations, was reportedly in the range of 10-15 %.

3.7 Concluding Summary

From the presented results, we can draw the following expectations and conclusions for the further work.

As a flow passed beneath the moonpool, the water column becomes excited by some frequency that increases in par with the velocity. When this excitation frequency is close to the natural frequency of the water column, the vertical piston-mode oscillation can be expected. The system locks into the natural frequency similar to the lock-in phenomena. As the excitation frequency grows we see a linear growth in the oscillation amplitude, until a sudden drop in the piston mode amplitude. Finally, the resistance acting on the hull due to the moonpool, consists of a base resistance that can be assumed to be constant, and a secondary term that is linearly connected to the oscillation amplitude.

Chapter 4

Modelling of the Moonpool Oscillations

4.1 Introduction

Now that we have built an impression of the phenomena related to the moonpool on a vessel during forward speed, we will now start to build a mathematical description of the motions observed.

We start by recalling Equation 2.9 which describes the equation of motion for the piston mode within a moonpool. To utilise this formulation we need to quantify the excitation force and the coefficients.

4.2 Moonpool Excitation Forces

The moonpool excitation forces can be decomposed into two different cases as shown in Figure 4.1. Primarily as a resonance problem due to a vertical oscillation of the hull, or due to vortex shedding as the flow streams over the moonpool edges. Needless to say, both cases might occur simultaneously.

(a) Resonance due to vertical oscillation   (b) Flow over a moonpool opening
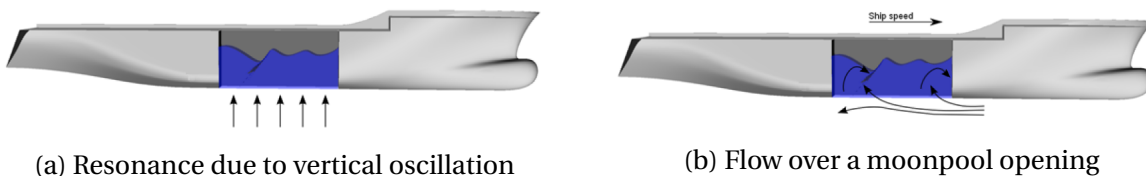
Figure 4.1: Moonpool excitation forces, adopted Hammargren and Törnblom (2012).

The resonance problem is a well investigated problem that is called gap resonance in the literature. This is a problem that has draw its attention in the context of the gap between ship-ship or ship-harbour configurations. Either-way, the physics remains the same, a confined water column that is exposed to the free-surface.

As a hull moves through the water, a flow is created over the moonpool opening. The water inside of the moonpool moves with the hull velocity, and as a consequence the free-flow will experience a discontinuity in the velocity as it flows over the leading edge of the moonpool. This discontinuity is a source for the creation of vortices, see Figure 2.2.

How these vortices are connected to the excitation force has been a source for discussion, or confusion in the literature. We have already mentioned the connection to the gap resonance, but there exists another analogy that can be seen in the literature. Turbulent flows over a closed cavity will be able reproduce some of the effects that are explained in the previous chapter.

The main problem behind closing the top of the moonpool is that this alters the physics of the problem. As long as the water column is exposed to the free-surface the stiffness is due to this exposure and the pressure on the mean free-surface. The moment one close the moonpool, this exposure is removed and the remaining stiffness comes from the compressibility of the fluid.

We will dedicate one section to the closed cavity analogy, before returning to the gap resonance. It is already explained why this analogy is unphysical, but we will illustrate how deep the rabit hole one can go.

4.2.1   Turbulent Flow over a closed Cavity

The flow beneath a hull is turbulent and as a consequence the inflow at the cavity will have a boundary layer. As the flow passes the leading edge, the discontinuity in the velocities creates a free shear layer. When the free shear layer hits the rear wall, the vortices collapses and the resulting pressure field interacts with the leading edge. This interaction is called impinging shear layers. The principal elements of self-sustaining oscillation of turbulent flow past cavity is illustrated in Figure4.2.
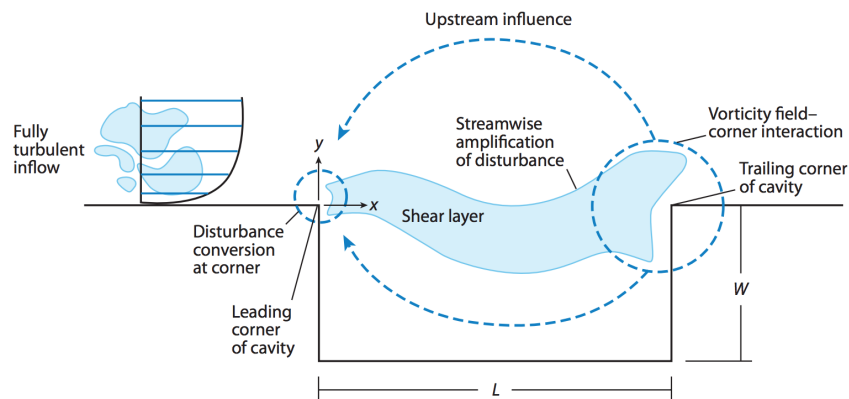
Figure 4.2: Principal elements of self-sustaining oscillation of turbulent flow past cavity, Rockwell et al. (2003).

The later phenomena is connected to edge-tones, which is a source of flow noise and undesirable structural loadings. Especially has this problem been investigated in the connection to among others, aircraft components, flumes and valves (see Rockwell and Naudascher (1979) and Naudascher and Rockwell (2012)).

Impinging shear layer problems bears the characteristics of frequency lock-in as the resulting resonance are in distinguished tones. In Figure 4.3a the two modes of resonance for a cavity with a turbulent boundary layer excitation is illustrated. The Strouhal number is illustrated as a function of the ratio between the boundary layer thickness compared to the length of the cavity. Sverre Steen (2013) gives the following approximation for the boundary layer thickness on a vessel.

$$\delta = 0.022034(\frac{3n+n^2+n}{n})^{\frac{6}{7}}Re^{\frac{-1}{7}}x \qquad \text{where} \qquad Re = \frac{Ux}{\nu} \qquad (4.1)$$

Where Re is the Reynolds number of the flow for the characteristic length and n is a integer chosen to be close to the logarithm of the Reynolds number. For our conservative case we will assume that the a vessel velocity of 5.14 m/s (10kn) and that the hull spans 50 meters from the fore perpendicular to the cavity opening. This gives a Reynolds number that is in the order of $10^{8.4}$, thus we chose a n equal to 8. The end result is a expected boundary layer thickness at the cavity opening that is 0.584 meters.

The goal of this small discussion is to present the development of the frequency of oscillation for a moonpool. Utilising the results from van 't Veer and Tholen (2008) as represented in Figure 4.3b we can combine this with the assumption of a excitation force that is categorised with a constant strouhal number. The moonpool length is 12.8 meters and the boundary-layer-to-length ratio equals 0.046. Going back to figure 4.3a it is not easy to read a accurate Strouhal number, but for simplicity we chose $St = 0.4$.

By assuming that the Strouhal number is constant outside of the range of oscillations, we can combine these results into Figure 4.4. The solid blue line shows how the frequency of vortex shedding increases linearly with increasing velocities, the red horizontal line marks the natural frequency, and finally the blue dotted line is the frequency for the observed water column oscillations. The latter figure shows remarkable resemblance with the illustrates used to explained lock-in.

We will not dig deeper into this analogy since it is already stated that this does not model the correct physics. But it has been illustrated that the cavity resonance for turbulent boundary layer excitation, shows for remarkable resembles to the observations for the moonpool.
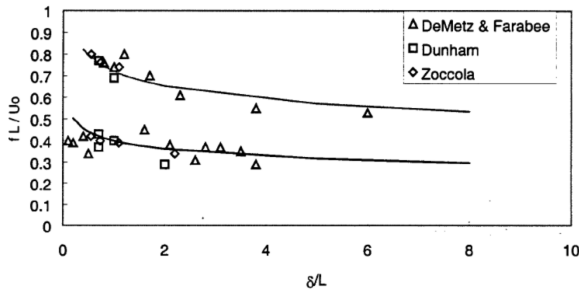
(a) Cavity Resonance Frequency for Turbulent Boundary Layer Excitation, Zoccola and Farabee (2001).
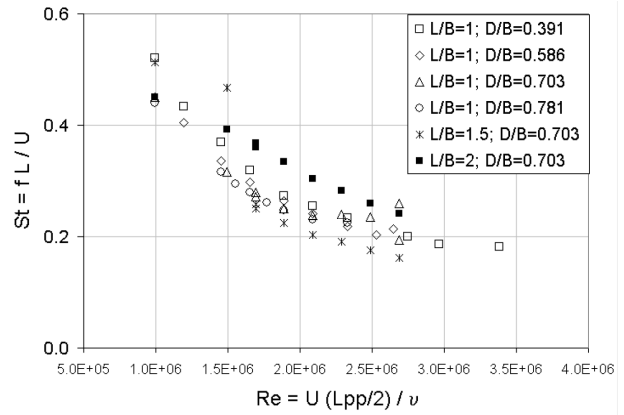
(b) Strouhal Number for piston-mode oscillation express by Reynolds number , adopted van 't Veer and Tholen (2008).

Figure 4.3: Cavity resonance analogy applied on a moonpool.
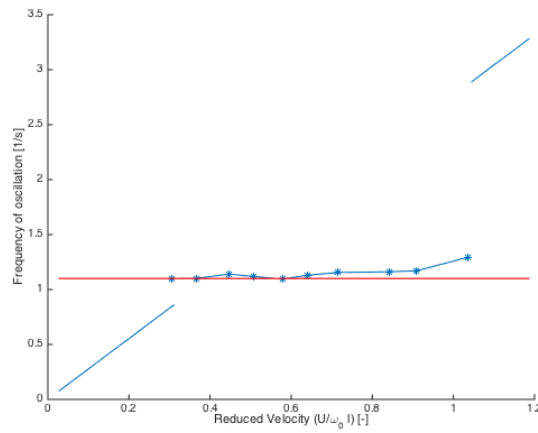
Figure 4.4: Frequency development for a moonpool given the cavity analogy.

4.2.2 Gap Resonance

As a flow passes over a edge or a step it is most likely to experience a discontinuity in the velocity. The differences of the fluid velocity on each side of the step, will due to viscosity cause a rotational effect on the fluid particles. This is illustrated in Figures 2.2 and 4.5, where we see that this rotation gives birth to a vortex.

The vortex develops with increasing flow velocity, until it sheds off the edge and continues downstream with the flow. The rotation is be counter-clockwise and will induce a negative pressure which in turn pulls downward on the water column.
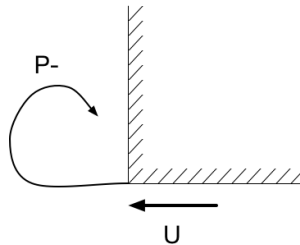
Figure 4.5: Vortex shedding at the leading edge at forward speeds.

With increasing flow velocity it is expected that the strength of the vortices and the related shedding frequency increases. Given sufficient strength, a vertical oscillation of the water column can be expected as the shedding frequency is in the proximity of the natural frequency. The oscillation alters the flow regime at the edges and becomes the dominating contribution to the vortex shedding. This can be used in explained the observed lock-in phenomena of the oscillation frequency.
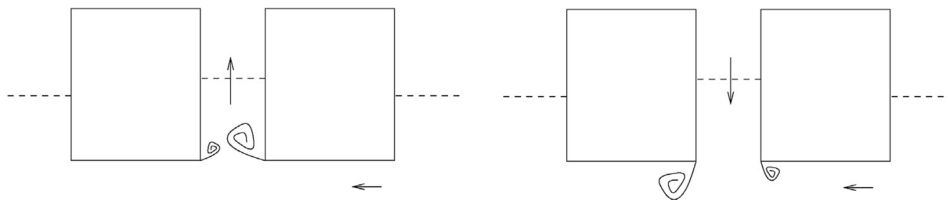
Figure 4.6: Asymmetrical shedding at the moonpool opening during oscillation, adopted Fredriksen et al. (2014).

In the work of Kristiansen and Faltinsen (2008) it was showed that the boundary layer at the in-flow can be neglected for all practical purposes.

4.3   Longitudinal and Transverse Motions - Sloshing Mode

Sloshing is a well known phenomena that takes place in almost any moving containment of a liquid with a free-surface. It is a complicated problem, but can often be modelled as a standing wave between two walls. Faltinsen and Timokha (2009) states that the excitation with frequencies within the vicinity of the lowest natural frequency is often of primary interest. However for our moonpool, the transient motions of the hull in surge and roll, and the disturbance from the vortex shedding at the leading edge is of importance.

In accordance to Newtons' third law of motion, as the hull is accelerated, the water within the moonpool experiences a opposite reaction acceleration, that forces the water to rise on the trailing wall. Mathematically in the xz-plane given as follows, see Çengel and Cimbala (2015).

$$\Delta y = \frac{a_x}{g + a_z} \frac{1}{2} l \tag{4.2}$$

The main damping component for sloshing inside of a moonpool is the viscous energy dissipation in the boundary layers of the walls. Needless to say, this makes sloshing long lived once excited.

4.3.1   Natural Frequency

The formulation for the natural frequency in sloshing in a 2D rectangular is by Faltinsen and Timokha (2009) given as following.

$$\omega_n = \sqrt{g \frac{n\pi}{l} \tanh(\frac{n\pi}{l} d)} \tag{4.3}$$

Here n is the mode of natural frequency, g the gravitational acceleration and l and d is the moonpool length and draft receptively.

Molin (2001) arrives to a similar expression through a quase-analytical approximation of the resont frequencies of a rectangular moonpool.

$$w_{n0} \simeq \sqrt{g \frac{n\pi}{l} \frac{1 + J_{n0} tanh(\frac{n\pi}{l} d)}{J_{n0} + tanh(\frac{n\pi}{l} d)}} \tag{4.4}$$

where J_0 involves an integral over the moonpool length and beam that can be obtained through numerical integration. The term J_0 is always lower then one.

4.4 Vertical Motions - Piston Mode

4.4.1 Natural Frequency

The water column oscillates in contact with the fluid below and thus added mass need to be considered. Recalling the definition of the natural frequency $\omega_0 = \sqrt{\frac{c_{33}}{m+a_{33}}}$, the added mass is the only unknown term in the expression. In the context of moonpools it is often written on the form of added draft; $d' = \frac{a_{33}}{\rho S}/$. A good place to start is with the recommendations from DNV (2011), as this also mathematically is the most flexible expression.

The natural frequency can be derived from the conseration of energy in system, $\frac{d}{dt}(E_k + E_p) = 0$. This leads to the follow expression for the undamped natural frequency:

$$w_0 = \sqrt{\frac{g}{\left\{\int_{-d}^{0} \frac{S(0)}{S(z)} dz + \frac{S(0)}{S(-d)} \kappa \sqrt{S(-d)}\right\}}} \tag{4.5}$$

The neat formulation from DNV (2011) includes the possibility for a cofferdam with an expansion of the cross-sectional area. In the DNV report it is stated the the κ has be found to be within 0.45 and 0.47 for rectangular moonpools with aspect ratio between 0.4 and 1.0. For a circular moonpool the parameter it is recommended to use 0.48. The report from DNV does not state any sources for this assumptions, but we will set κ equal to 0.47 since we are investigating square moonpools. Thus the added drought is expressed as $d' = 0.47l$

Both Knott and Mackley (1980) and Faltinsen (1993) derives the equations of motions from the Bernoulli equation. The added mass is neglected by considring the problem in on dimention in the work of Faltinsen, while Knott and Mackley comments on the problems related to the neglecting of these forces. Thus with a $\kappa = 0$ the natural frequency is reduced to $\omega = \sqrt{g/d}$.

Fukuda (1977) was one of the first authors to analyse the added mass term for the piston mode oscillation moonpool. He ran experiments with both rectangular and circular moonpools, and concluded that there are a linear connection between the added draft of the moonpool and the root of the cross-section area. His recommendation is a $\kappa = 0.41$ for all geometries, and this is higlighted in figure 3.2.

Berget et al. (2009) creates a rough approximation by taking the added mass of a flat plate oscillating in infinite water, which is $a_{33}^{2D} = \frac{1}{2}\frac{\rho \pi S}{4}[kg/m]$. Sadiq and Yao (2014) gets the same expression from evaluating the added mass for a half sphere covering the moonpool opening. Both methods yields a $\kappa = 0.39$.

Molin (2001) developed a quasi-analytical approximation of the resonant frequencies and corresponding modes. He assumed that the beam is much larger then the width of the moonpool and mimiced the outer free-surface by placing sinks at the of the hull at keel level, $(\pm B_T/2, -d)$. A note is that B_T needs to be slightly longer then the actual beam, as stated by Molin and shown

by Maisondieu and Ferrant (2003). In just two-dimensions he arrived to the follow expression:

$$\omega_0 = \sqrt{\frac{g}{d + \frac{b}{\pi d}(\frac{3}{2} + lnB_T)}} \tag{4.6}$$

In three-dimensions the expression becomes a somewhat more complicated.

$$\omega_0 = \sqrt{\frac{g}{d + d'(b, l)}} \tag{4.7}$$

Where the added draft is a function of length and beam of the moonpool and is given as.

$$d'(b, l) = \frac{b}{\pi}\left\{\sinh^{-1}(\frac{l}{b}) + \frac{l}{b}\sinh^{-1}(\frac{l}{b}) + \frac{1}{3}(\frac{b}{l} + \frac{l^2}{b^2}) - \frac{1}{3}(1 + \frac{l^2}{b^2})\sqrt{\frac{b^2}{l^2} + 1}\right\} \tag{4.8}$$

If we have a quadratic cross-section this long expression reduces down to $d' = 0.4732l$.

	Added draft
Faltinsen (1993)	0
Fukuda (1977)	$0.41\sqrt{S}$
DNV (2011)	$0.47\sqrt{S}$
Berget et al. (2009)	$0.39\sqrt{S}$
Molin (2001)	$d'(b, l)$

Table 4.1: Listing of the different approximations of the added draft.

As further illustrated by the listings in Table 4.1, there is a wide spread in the recommended values of κ. The conclusion that we can draw from this, it the one can in a early phase estimate the natural frequency based on DNV (2011), but it is needed to verify this frequency with experiments.

4.4.2 Damping

The damping of the system is of great interest since this is the forces that limits the amplitude of the piston-mode in resonant conditions. Figure 4.7 illustrated the difference between a linear theory and the results from experiments. From this figure, it is clear that the neglecting of viscosity does not does not yield reasonable results. The only component included is the linear damping, is related to the energy dissipated as waves radiates away from the hull.

The main damping component that comes from viscosity is relates to the fluid separation at the opening of the moonpool. As the water coulmn oscillates, vortices are shedded at the edges of the moonpool opening, as shown in Figure 4.8.
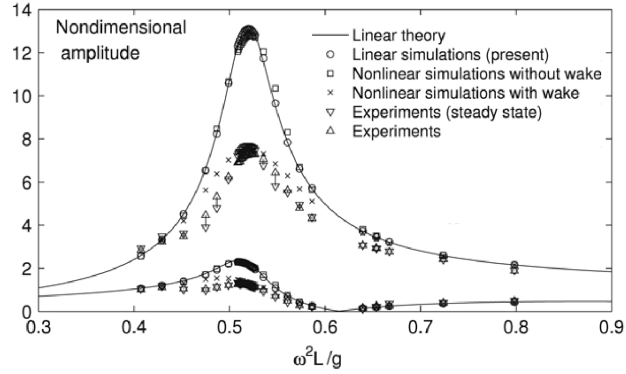
Figure 4.7: Non-dimensional amplitude of the piston mode in a gap as a function as a dimensionless frequency, adopted Kristiansen and Faltinsen (2008).

The mechanism of the vortex shedding in relation to a oscillation water column was investegated experimentally by Knott and Mackley (1980), and recently by Kristiansen and Faltinsen (2008). The former demonstrates mathematically how the eddy damping increases linearly with the amplitude-to-gap length ratio. A higher amplitude will introduce a higher velocity of the oscillation, and stronger vortices will be shredded of at the moonpool opening. Likewise is the damping factually strongest on the downstroke of the oscillation, as the vortices are disturbed by the limiting geometry in the upstroke.
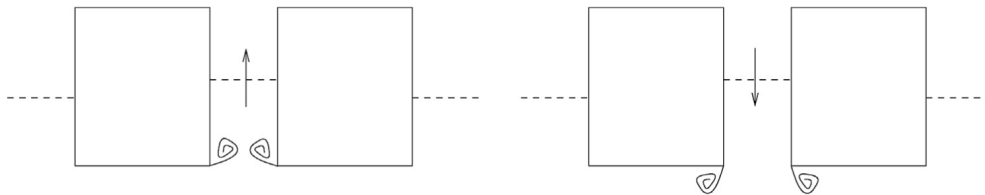
Figure 4.8: Symmetrical shedding at the moonpool opening during oscillation, adopted Fredriksen et al. (2014).

4.4.3   Prediction of oscillation amplitude

As a model for the moonpool piston-mode oscillation now has been established and the parameters has been quantified to some extent, it is possible mathematically predict the amplitude of the system. Recalling the full equation of motion for a single body in Equation 2.9, and divide all terms by ρS, we arrive to the following expression.

$$(d + d')\frac{d^2\eta}{dt^2} + b_1'\frac{d\eta}{dt} + b_2'\frac{d\eta}{dt}|\frac{d\eta}{dt}| + g\eta = \frac{F}{\rho S}$$

(4.9)

Here we have assumed a constant cross-sectoin and we arrive at the basis for the formulations found in Fukuda (1977). The mean level of the free-surface is described by $\eta(t)$ and it is deifned as zero at equilibrium, i.e $\eta = h\sin(\omega t)$. Fukuda then argues that there is a excitation force driving the water column only when the free-surface moves upwards from the equilibrium level, and has a positive velocity upwards. This force is quantified to be $F(t) = \rho S\frac{d\eta}{dt}V_e(t)$. Notice that the first part $\rho S\frac{d\eta}{dt}$ equals the mass flux that is entering the moonpool at any given time t. Mathematically these assumtions can be written as the following expressions:

$$(d+d')\frac{d^2\eta}{dt^2} + b_1\frac{d\eta}{dt} + b_2\frac{d\eta}{dt}|\frac{d\eta}{dt}| + g\eta = V_e(t)\frac{d\eta}{dt} \qquad \eta \geq 0 \qquad \frac{d\eta}{dt} > 0$$
$$(d+d')\frac{d^2\eta}{dt^2} + b_1\frac{d\eta}{dt} + b_2\frac{d\eta}{dt}|\frac{d\eta}{dt}| + g\eta = 0 \qquad\qquad \eta < 0 \qquad\qquad\qquad (4.10)$$

Then by the means of energy conservation through an oscillational cycle the amplitude h can be expressed.

$$h = \frac{3\pi}{16}\frac{V_e - 4b_1}{2b_2\omega} \qquad\qquad (4.11)$$

In order to simplify this expression, Fukuda connects the velocity in the excitation force with the flow velocity. By conservation of mass the flow velocity can be decomposed into two sub components, $mU = m(V_e+V_c)$. This is further utilised to define a onset velocity $U_{onset} = V_c+4b_1$. By definition, the oscillations starts to be observed at this velocity.

$$\frac{h}{l} = \frac{3\pi}{16}\frac{U - U_{onset}}{(2b_2)\omega_0 l} \qquad\qquad (4.12)$$

The second order damping coefficient b_2 is defined as the half of the squared ratio between the cross-section area at the free-surface and the keel, $b_2 = \frac{1}{2}(\frac{S_{top}}{S_{bottom}})^2$. For a clean moonpool this reduces to $b_2 = \frac{1}{2}$, and only $\omega_0 l$ is left in the denominator Equation 4.12.

The latter equations gives a linear growth of the amplitude which has been proven to show similarities with the experimental results. As we can recall from the earlier Figure 3.4, the linear increment of $3\pi/16 \approx 0.589$ given a good agreement with the experimental results. The current expression does however lack further formulations for the onset and offset velocities.

Based on the existing experimental results it is possible to see a trend towards a onset velocity that can be defined as $U_{onset} = 0.35\omega_0 l$. The offset velocity however seem to be more related to each individuacal case, but are to be found in the velocity range of $U' \in [0.6, 0.8]$.

Chapter 5

Resistance due to the Moonpool

5.1 Introduction

In the previous presentation of the exsisting experiment data, it is assumed that the resistance due to the moonpool can be expressed as a linear function of the oscillation amplitude. That is, a constant term that rises from the existence of the moonpool, and a linear term that increases as the oscillation amplitude grows. This trend is reported by among others van 't Veer and Tholen (2008), as shown in figure 3.6b.

In the literature the resistance is defined by a resistance coeficent based on the cross-secional are of the moonpool.

$$C_{\Delta MP} = \frac{\Delta R}{\frac{1}{2}\rho S U^2} \tag{5.1}$$

In this chapter the components of the resistance will be discussed, before a list of measurements in order to reduce this resistance is presented.

5.2 Base Resistance

The moonpool is a great modification on the hull from both a structural and hydrodynamical point of view. The opening beneath the hull changes the flow drastically and it can safely be assumed that the influence on the resistance is negative.

Kristiansen (2006) conducted a towing test on a model of the IMR vessel that today bears the name Edda Fauna. This is a ship that is 109 meters long and it is based on the ST-225 design from Skipsteknisk, DeepOcean (2008). As already mentioned the velocities where so high that no considering oscillation was observed. Scaled up to full-scale velocities the towing test were ran at 12-18 knots, and the reported increase in resistance was 5,8-6,2 % (increasing with velocity). A maximum velocity of 18 knots is a bit high for the majority of the offshore velocities of interest,

but to be able to define quantify the resistance to 6 % in the velocity range 12-14 knots is of great interest.

During conversations with different players in the offshore industry, it seem to be e established rule of thumb that the resistance due to the moonpool is in the magnitude of 10 %. It is assumed by many that the moonpool placement and the hull in general plays a great role in this number.

Other findings in the literature does not express this area of the study in clear text. The base resistance can however be estimated from the enclosed figures. Fukuda (1977) shows for a resistance in the magnitude of 5-10 % for a model with a circular moonpool (L=4 m, 2R = 0.093 m, d = 0.093 m). Cotteleer (2000) illustrates a mangitude of 5-15 % for their drillship model with a square moonpool (L=4.2 m, l=0.256 m, d=0.179 m).

Kristiansen (2006) states a hypothesis in his master thesis, that the base resiatnace can be calculated from the base drag. This drag component is commonly used for bluff bodies and therefore the transom stern on vessels. The drag is connected to the separation at the rear end of the body.

$$C_{\Delta MP} = C_{Base} = 0.029 \frac{(S_{base}/S)^{\frac{3}{2}}}{\sqrt{C_{FS}}} \qquad \text{where} \qquad C_{FS} = \frac{0.075}{(log(Re) - 2)^2} \qquad (5.2)$$

Where S_{Base} is the base area that equal the moonpool width time the draft, S is the wetted surface of the hull in front of the moonpool. And C_{FS} is the frictional coefficient and is dependent on the Reynolds number for the vessel. Kristiansen gets a agreement with a deviation of 10-15 % from his experimental values. From a physical point of view this drag coefficient neglects the influence of the rear moonpool, and these results might as well be a coincidence. In this work it was not found any literature were the wetted surface of the vessels were given, thus insufficient data to reproduce this results for different models.

5.3   Resistance due to Oscillations

With oscillations present, the resistance was observed to vary with the same frequency. This leads to the assumption that they are directly connected to each other.

In Fukuda's formulations for the equations of motions, the resistance can be evaluationed by time avraging the excitaion force over one period. This force was expressed as $F = \rho S \frac{d\eta}{dx} V_e(t)$, where $V_e(t) < U$ is the velocity entering the moonpool. By conservative letting $V_e(t) \rightarrow U$, the resistance can evaluated as the following integral.

$$\Delta R = \frac{1}{T}\int_0^{T/4} \rho S \overbrace{(h\omega cos(\omega t))}^{d\eta/dt} U \mathrm{d}t = \frac{1}{2\pi}\rho SUh\omega \tag{5.3}$$

$$C_{\Delta MP} = \frac{\Delta R}{\frac{1}{2}\rho SU^2} = \frac{1}{\pi}\frac{\omega h}{U} = \frac{1}{\pi}\frac{\omega l}{U}\frac{h}{l} \sim 0.3183\frac{1}{U'}\frac{h}{l} \tag{5.4}$$

Note here that the terms $\rho S\frac{d\eta}{dx}$ equals the mass flux entering the moonpool, thus a similar results is reached by evaluating the change of momentum in the water-column. The results from both English (1976) and Fukuda (1977) gives a somewhat good agreement with this approach, as seen in Figure 3.5.

In the Dutch campaigns of Cotteleer (2000) and van 't Veer and Tholen (2008) the results were evaluated in order to build a linear model between the resistance and the oscillation amplitude, as shown in the Figures 3.6. van 't Veer and Tholen concludes with the following linear connections, depending on the dominating mode of oscillation.

$$C_{\Delta MP} = 0.3625\frac{h}{l}\frac{l}{d} + 0.01474 \qquad\qquad \text{Piston-Mode} \tag{5.5}$$

$$C_{\Delta MP} = 0.1720\frac{h}{l}\frac{l}{d} + 0.03587 \qquad\qquad \text{Sloshing} \tag{5.6}$$

In order to compare the coefficients against each other, it is assumed that amplitude development follow the formulation of Fukuda in Equation 4.12 with a onset velocity of $U'_{onset} = 0.35$. The moonpool had a geometric ratio $d/l = 0.7$, which is the most common draft in the Dutch campaigns. The constant terms were neglected since we only considered the resistance from the oscillations.

Considering that the oscillations were observed in most experiments within the range of $U' = [0.35, 0.8]$, it is clear that the formulations of Fukuda (1977) and van 't Veer and Tholen (2008) for the piston-mode aligns. The sloshing-mode results in a lower resistance, as expected due to the linear term that is 47% lower then for the piston-mode.
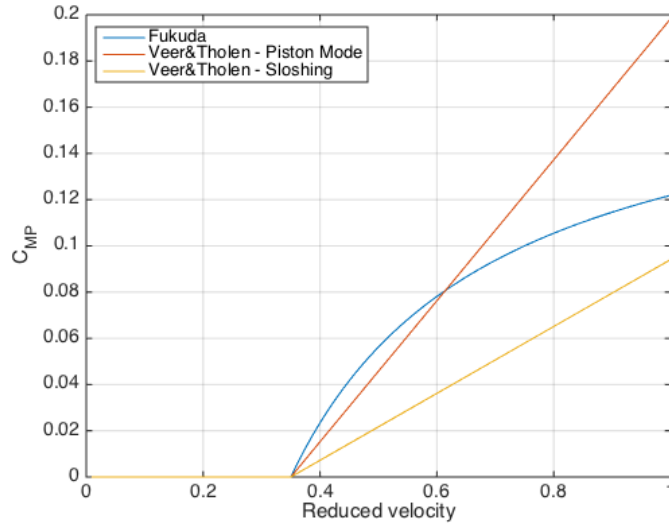
Figure 5.1: Moonpool resistance coefficient over the reduced velocity.

5.4   Measures to reduce the Resistance

In this section we will present a short summary of the different measures mentioned in the literature in order the minimise the resistance due to the moonpool. The suggestions are divided into two categories; system alterations and decrease of the excitation force. In the former category the focus is mainly on increasing the damping of the system, while in the latter category most suggestions seek to alter the flow over the opening in a beneficial matter.

5.4.1   Alteration of the System

Damping Plates & Chambers

The simplest form of damping can be achieved by installing damping plates on the inner walls of the moonpool. These are also named choke deck and are in practice simple appendages or flanges. Early works of both Fukuda (1977) and Aalbers (1984) shows for a increase of the damping of the system and that the ideal vertical position for a single damping plate is just a small distance below the mean free-surface.

Figure 5.2a illustrates how the damping chamber basically is an expansion of the moonpools cross-section. Bulkhead walls are shown in the figure as dotted lines. The bulkheads serves for two reasons; firstly they act as a guidance system in order to avoid hitting the sharp edges at the opening during lifting-operations, and secondly they are perforated such that they dampen the horizontal sloshing as well. As illustrated in the earlier figure 1.2b, the void inside of the damping chamber is normally equipped with a number of chokes decks to further dampen the vertical oscillation.
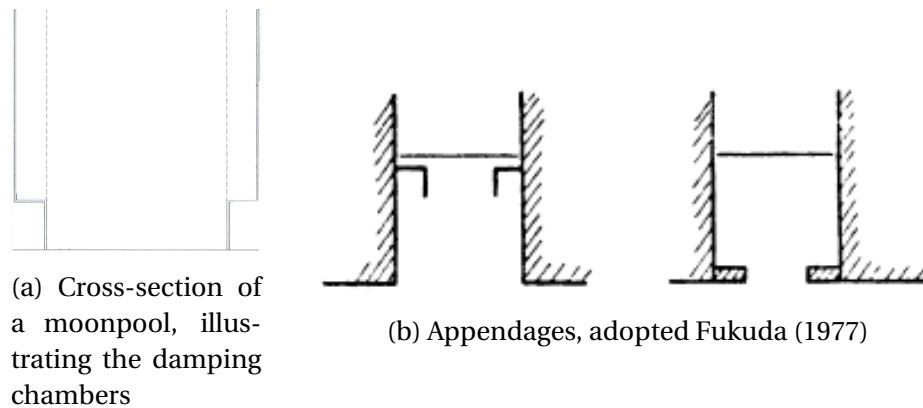
(a) Cross-section of a moonpool, illustrating the damping chambers

(b) Appendages, adopted Fukuda (1977)

Figure 5.2: Illustrations of damping chambers, perforated bulkheads and choke decks inside a moonpool.

Closing of the moonpool

Closing of the moonpool below the free-surface will change the physics of the system by removing the exposure to the atmosphere. The problem changes to a cavity flow and naturally the oscillations vanishes, but also the base resistance can be assumed lowered.

The moonpool can also be enclosed above the free-surface, as this will create a air-cushion that contributes with stiffness. Gaillarde and Cotteleer (2001) states that by closing the top of her model, the vertical oscillations vanished completely. A note here is that a air-cushion like that can be considered to be incompressible in model scale, while in full scale the compressibility needs to be considered.

5.4.2 Decrease of the Excitation Force

Wedges, cut-outs and foils

Inspired by the related works done on closed cavities, the classical proposal is to alter the flow at the edges of the moonpool opening. The thought is that wedges and cut-outs reduces the vortex creation, while a foil will alter the flow in a beneficial way.

In the existing literature there are a number of authors that have to some extent investigated a related solution. Various suggestions are illustrated in Figure 5.4. The latter figure is taken from Kristiansen (2006), and his conclusions highlights the problems related to this measures. As these suggestions aim to alter the flow over the moonpool opening, there will exists a related ideal angle for a given velocity. Since the flow under hull is highly unsteady, it possible to argue that a solution wit a fixed angle can have a negative effect. In fact, of the eight suggestions shows in Figure 5.4, only alternative (*g*) proved to have any positive effect on the resistance.

Grid of Flaps

A grid of flaps has accordingly to several authors proven to be a prominent solution. This is also the only suggestion that was found to be commercially available. Parosha, a Dutch company, provides a moonpool door that consists of grid of flaps as shown in Figure 5.3a. The door is hatched in the bottom of the moonpool, and can be hoisted by a crane such that it folds into and becomes a part of the damping chambers. On the company website [1], one can read that this door is installed on a handful offshore construction vessels. An attempt to reach out to the company was conducted, but the details of their solutions was supplemented with a nondisclosure agreement.

The US Patent 8,770,124 B2 - "Device for diminishing flow resistance in moon pool" by Choi (2014) from Daewoo Shipbuilding & Marine Engineering Co LTD, describes a similar solution. In the patent it is possible to graphically interpret a reduction of the power consumption of the magnitude of 15% by using their product.

Gaillarde and Cotteleer (2001) conducted a interesting test where they used this arrangement to only cover the rear half of the moonpool in order the reduce the water up-flow. The results from both cases shows for identical results in terms of resulting oscillations and resistance.
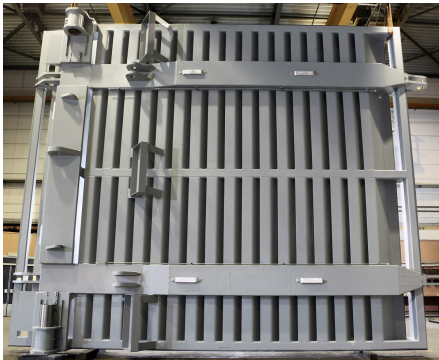
(a) Door with a grid of flaps, adopted Parosha
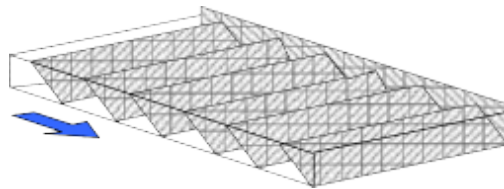
(b) Illustrations of a grid of flaps, adopted Gaillarde and Cotteleer (2001).

Figure 5.3: Grid of flaps

---

[1]Webpage   accessed   08.06.2015   `http://www.parosha.com/our-innovations/offshore-maritime/moonpool-door/`
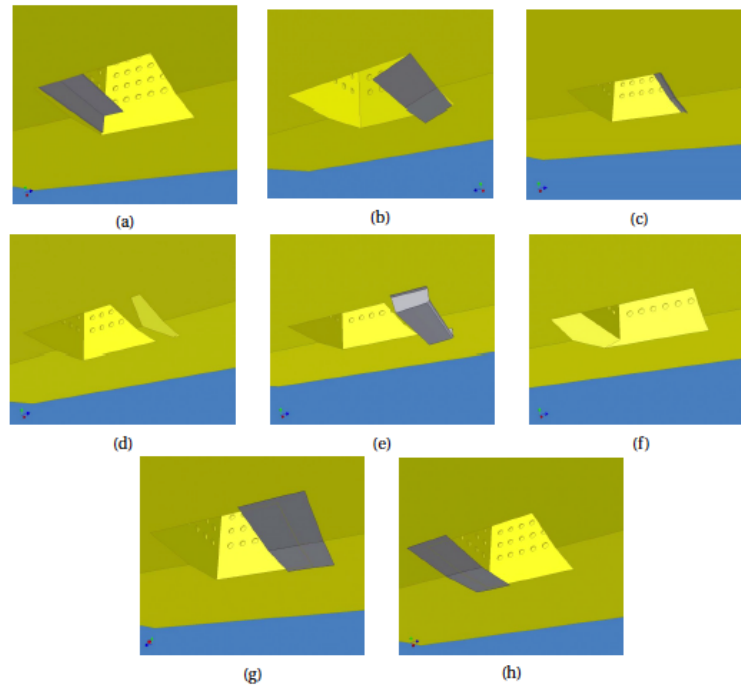
Figure 5.4: Suggested measures in order to alter the flow over the moonpool, Kristiansen (2006).

Part III

Numerical Simulations

Chapter 6

Computational Fluid Dynamics

6.1 Introduction

Computational Fluid Dynamics (CFD) is a common denominator for the use of numerical methods to solve and analyse fluid flows problems. In this chapter a short introduction to the topic will be given, but for further investigations on the topic recommendations goes to the enormous list of published work, e.g. Ferziger and Peric (2001) or introduction chapter on CFD in Çengel and Cimbala (2015).

The process of a CFD analysis is normally divided into the following three parts; *pre- processing, solving* and *post-processing*. The *pre-processing* is often the most challenging part, and in many ways it can be said that several aspect of this part is a craftwork where experience is the keyword. First and foremost it is necessarily to understand the physics of the problem that is to be modelled, and to be able to create a conceptual mathematical model. Once the forces involved in the problem is understood, it is possible to further define a mathematical of a grid of cells within a constrained domain.

In the *solver* part, the governing equations are solved or approximated within each of this mathematical cells. This grid of cells are also referred to as a mesh and is directly connected to the computational time of a simulation. With decreasing number of cells, the computational time also decreases, but you run the risk of not being able to capture the physics in the problem correctly. All these arguments regarding physics and computing time, emphasises the importance of the *pre-processing*. The final *post-processing* usually involves a range of softwares to visualise and present the results from the solver.

6.2   Mathematical Description

6.2.1   Governing Equations

The cornerstone of any CFD analysis procedure is the fundamental governing equations of fluid dynamics, i.e. the continuity, momentum and energy equations. These are the equations that model the physics in the analysis. For a viscous fluid flow the Navier-Stokes equations are used to assure conservation of momentum. Note that the energy equations are only included when the development of the temperatures are of interest.

The two-dimensional Navier-Stokes equations for an incompressible fluid can be written as.

$$\frac{\partial u}{\partial t} + u\frac{\partial u}{\partial x} + w\frac{\partial u}{\partial z} = -\frac{1}{\rho}\frac{\partial p}{\partial x} + v(\frac{\partial^2 u}{\partial x^2} + \frac{\partial^2 u}{\partial z^2}) + f_x \tag{6.1}$$

$$\frac{\partial w}{\partial t} + u\frac{\partial w}{\partial x} + w\frac{\partial w}{\partial z} = -\frac{1}{\rho}\frac{\partial p}{\partial z} + v(\frac{\partial^2 w}{\partial x^2} + \frac{\partial^2 w}{\partial z^2}) + f_z \tag{6.2}$$

Along with the requirement of continuity of mass,

$$\frac{\partial u}{\partial x} + \frac{\partial w}{\partial z} = 0 \tag{6.3}$$

In a Cartesian coordinate system (x,z), u and w are the x- and x-components for the fluid velocity, t is the time and p is the pressure. ρ is the mass density of the fluid , v is the kinematic viscosity coefficient and f is the external force acting on a fluid particle. For most purposes, the only external force acting a particle is the gravitational acceleration, i.e. $f_z = g = 9.81 m/s^2$.

6.2.2   Domain and Grid

Once the physical problem is described as a mathematical model, the goal of the CFD analysis is to simulate a flow problem within a geometrical region of interest that is called the domain. Within this domain we then need to create set of cells in which the flow variables will be calculated. This collection of cells is called a grid or a mesh.

A two-dimensional structured grid consists of planar cells with four edges within a rectangular domain, i.e. the cells have a rectangular shape. This is the simplest type of grid, and is mathematically simple because all cells in the same row or column share at least one length attribute. An unstructured grid on the other hand does not require a length similarity between each cell, thus all sides of a cell might be stretched independently. This allows for the use of triangular and rectangular shapes that can be stretched into any arbitrary shape.

The domain itself is often divided into multiple blocks with different grids. This is called a multi-block analysis and follow the simple philosophy that it is beneficial to have a dense mesh

in the area of main interest, while in the far-fields of the domain the mesh can be coarser.

6.2.3 Numerical Schemes

The governing equations are essentially a set of partial differential equations, which needs to be transformed by discretization into a set of algebraic equations that can be solved. The three most common methods to do this discretization is; the Finite Difference Method, the Finite Volume Method and the Finite Element Method. For CFD related problems, the Finite Volume Method is the most common method of choice.

For unsteady flows it is also necessarily to select a numerical method in order to process in time. In relation to the Finite Volume Method, the most common time schemes are Euler and Crank-Nicolson.

6.2.4 Time-Step Size

The Courant Fridrichs Lewy number (CFL), or just Courant number for short, condition states that for a given grid, the time step cannot be bigger then some quantity depending on the numerical schemes.

$$CFL = \frac{u\Delta t}{\Delta x} \tag{6.4}$$

It is normal to define a requirement that the Courant number needs to be less or equal to unity, Physically this assures numerical stability by requiring that the information does not progress more than one cell during a time step. However in an unsteady analysis it is normal to require a Courant number much lower in order guarantee stability as the velocities develop over time.

For a free-surface boundary condition there exits a second stability criteria that can be used. Dommermuth and Yue (1987) shows how the following criteria can be obtained by stability analysis of the fourth-order Runge Kutta scheme.

$$\Delta t \leq = \frac{8}{\pi} \frac{\Delta x}{g} \tag{6.5}$$

We were not able to similar criteria for different types of time-schemes.

6.2.5 Boundary and Initial Conditions

Appropriate boundary conditions are required in order to obtain a stable numerical solution that is able to capture the physics in a problem. In this section, the boundary conditions utilised in the later simulations are to be presented.

Inlet & Outlet

Inlet and outlet are the names given to patches were the fluid enters or leaves the domain. It is of importance that these boundaries are situated far away as possible from the region of interest, in order to not numerically interfere with the physics. Common practice is to predefine the mass flux and a reference pressure at the inlet, and to require a zero gradient for the fluid variables on the outlet.

Wall

A body within the domain or a restricting wall patch of the domain, might share the wall boundary condition. For the fluid the wall is impermeable, and due to the no-slip condition the fluid sticks to the wall. On general form this is expressed simply as:

$$\vec{U} = \vec{U}_{Wall} \tag{6.6}$$

Where U_{Wall} is the wall velocity, and for a fixed wall the implementation is simply $U_{Wall} = 0$.

Free-Surface

The free-surface boundary condition is linearised and applied on the mean free-surface. This condition has proven to be sufficient as long as the waves modelled on the free-surface have small amplitudes and are linear.

$$P = g\zeta \qquad and \qquad \frac{\partial \zeta}{\partial t} = -U_1 \frac{\partial \zeta}{\partial x} - U_2 \frac{\partial \zeta}{\partial y} + U_3 \qquad on \qquad z = 0 \tag{6.7}$$

For problem regarding the interaction between linear wave-induced motions and linear waves, and the absent of forward speed and currents, several terms vanishes and simplifies the expression, as shown by Faltinsen (1993).

$$P = g\zeta \qquad and \qquad \frac{\partial \zeta}{\partial t} = U_3 \qquad on \qquad z = 0 \tag{6.8}$$

Symmetry & Slip

A symmetry boundary forces the flow variables to be mirrored about a plane of symmetry. This requires mathematically that the normal velocity is zero, and that the normal gradients for all

flow variables are zero on the symmetry plane. The free slip condition requires a zero gradient for the tangential velocity components, and zero value for all non-tangential velocities.

6.2.6   Implementation of the Free-Surface in CFD

For fluid problems that handle the free-surface, it is a field of great interest how to beneficially model the interface between the two fluids. The problem is illustrated in Figure 6.1, where we see three different solutions that captures the fluid interface.

The traditional solution of a one-fluid formulation is shown in Figure 6.1b. The fluid density and viscosity varies in space, and the fluid distribution in the domain is keep track of by a marker-function. The mayor downside with this tactic, is that it require a dense mesh in the interface and is considered to in general computationally expensive.
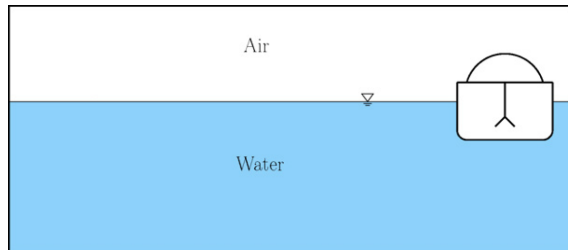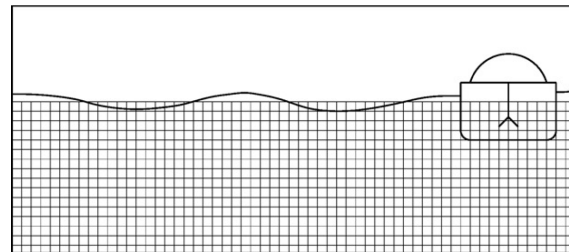

(a) Sketch of a numerical wavetank
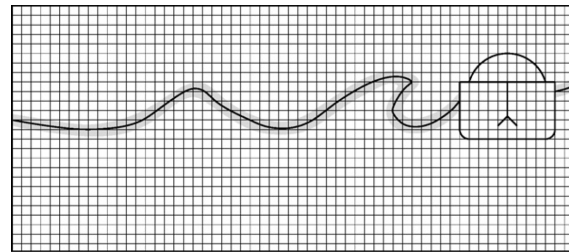
(b) One-Fluid formulation, smoothed interface between air and water.
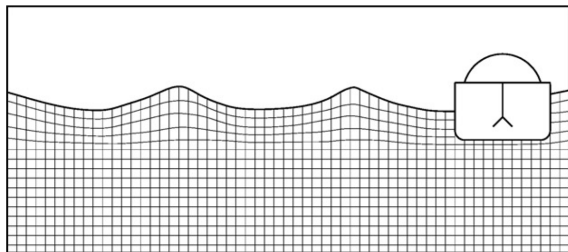
(c) Sharp interface, geometry conforming grid

(d) Fixed domain, pertutbation of potential

Figure 6.1: Tactics for the wavetank domain decomposition, adopted Kristiansen and Faltinsen (2012).

Another approach that seeks to reduce the computational expenses it a boundary fitted grid, as shown in Figure 6.1c. Now the problem is reduced to only include the water, and the interface is tracked by the grid. In each time-step were the fee-surface moves, the coordinates of the cells in the boundary are adopted. The disadvantages are that the domain becomes highly complex and special attentions needs to considered in the set-up each case. This solution remains somewhat computational heavy.

The final approach that will be considered in this text, is the hybrid approach, shown in Figure 6.1d. The domain is remains fixed, and the free-surface is modelled using potential flow

formulations. This approach require a clear physical understanding of the problems at hand, and it is considered to be magnitudes less demanding computational-wise due to the fixed domain.

6.3   Error Sources

In the use of numerical methods and modelling it is important to be aware of the different layers of error that might occur. Some of these errors are user-based and are related to the conceptual model and choice of solutions methods, while other errors are simply numerical error within the solutions methods. The user-based errors can sometimes be easy to improve and can often be what separates an experienced and inexperienced CFD-user. The numerical errors are on the other hand bound to the methods in the solver, but it is important to be aware of these layers of errors. Figure 6.2 illustrates the different layers of error that are to be expected in a CFD analysis.
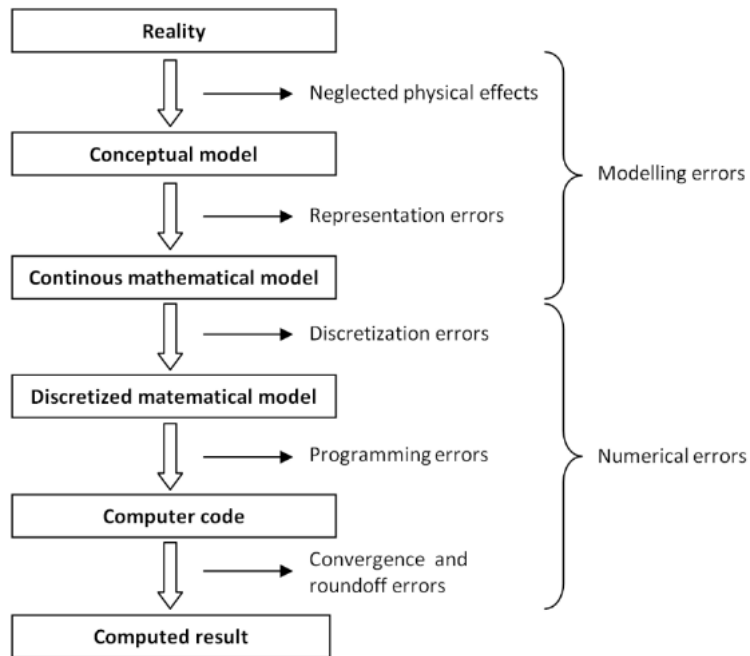
Figure 6.2: Sources of errors in CFD analysis (Hammargren and Törnblom (2012), adopted from Larsson Lars (2010)).

6.4   OpenFOAM & PVC3D

OpenFOAM (Open-source Field Operation and Manipulation) is a open-source toolkit for the development of numerical solvers. The toolkit is written in the programming language C++ and it is in principle system independent, but the only official maintained distribution is for

linux based systems. By default the OpenFOAM installation also includes a number of prebuilt solvers and both pre- and post-processing utilities. This leads to some confusion connected to the name OpenFOAM as both a solver-package and as a programming toolkit. OpenFOAM does not come with a traditional user manual, both rather is all the solvers and utilities explained in different tutorials.

Being a open-source toolkit the focus of OpenFOAM and the experience in the use of Open-FOAM, is that all aspects of the data is highly accessible. Each OpenFOAM case consists of a folder, containing a minimum the following three sub-folders.

- **system** directory that contains files for setting parameters associated with the solution procedure.
- **constant** directory containing a full description of the mesh and files that specifies the physical properties of the case.
- **0** directory containing files that defines the initial and boundary conditions.

All case parameters that are necessary for a solver is saved normally in plaintext files within these three sub-folders. There exists some projects that provides graphical user interfaces for use of OpenFOAM, but the common method is to edit files from a editor and running codes from the command line interface.

PVC3D (Potential Viscous Code 3D) is a in-house MARNITEK code, that has been developed with support from Statoil RDI, and is based on a hybrid method that combines viscous flow with boundary conditions from potential flow. In this solver the Navier-Stokes equations are discretised using Finite Volume Method. The Euler method is utilised to march the solution forward in time.

The unique part of this solver is the capacity to introduce the linear free-surface condition of the free-surface, and utilise this to keep track of the water elevation. This has been proven to be sufficiently good for problems where the waves are of small amplitudes and of linear nature.

The PVC3D package is currently under development and thus has been, and is, under several validation and verification studies for different related flow problems. Gap resonance has been investigated in Kristiansen and Faltinsen (2012), and heave for three-dimensional moonpools in Kristiansen et al. (2013).

Chapter 7

Simulation Campaign

7.1 Introduction

As discussed in Chapter 3.7 the resistance components can be decomposed into the constant base resistance and a oscillating term that is connected to the water oscillations within the moonpool.

The goal of the current investigation is to simulate the vertical water oscillations as they develop over a range of velocities. The fields of interest for the analysis is to define the onset and offset velocities, the rate of growth as predicted in equation 4.12 and finally to attempt to analyse the forces that acts on the hull.

In order to benchmark the numerical results against experimental data, a case from the campaigns of van 't Veer and Tholen (2008) was selected. This case and the details of the experiment is presented in the following section.

7.1.1 Dutch Experimental Campaign

The campaigns of van 't Veer and Tholen (2008) and Cotteleer (2000) were conducted on a 1:50 scale model of a drillship. In the paper of van 't Veer and Tholen the case that was easiest to extract the results from the figures was chosen, and the piston mode development is reproduced in Figure 7.1. The case is based on a square moonpool, with a draft-to-length ratio of 0.7. In model scale this gives a hull that is 4.2 meters long, draft of 0.1792 meter and a square moonpool of 0.256 x 0.256 meters.

The data that we seek to reproduce is the non-dimensional amplitude over a range of velocities. From the paper we can read that each data point represents the significant moonpool resonant amplitude. And that this value was obtained by averaging the water elevation inside of the moonpool over a time-series. In their towing tests, the recordings of the water level was started when the motions reached its observable peak level and that the recording time was 60

seconds. The observed oscillation had a frequency in the range of 0.9 - 1.1 Hz, thus we can assumed that a total of 60 amplitudes were observed during this 60 seconds sampling window.
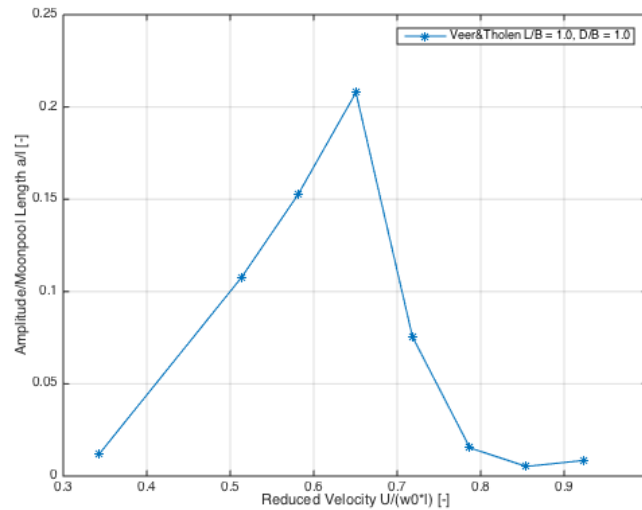

Figure 7.1: Piston mode water oscillation amplitude as a function of the reduced velocity, reproduced from van 't Veer and Tholen (2008).

The experiments was conducted at the Towing Tank I at the Delft University, which has a length of 142 meters. The models was tested up velocities of $1,7$m/s, $U' \approx 1.1$, thus given the 60 seconds sampling window, the length of the towing tank is clearly a limitation factor.

7.1.2 General Assumptions and Remarks

The numerical set-ups and main ideas as highly inspired from the earlier works on moonpool with PVC3D, see Fredriksen (2015).

The meshes is to be generated by the OpenFOAM utility *blockMesh* in order to produce multi-block grids with hexahedral cells. This utility produces a mesh that spans in all three-dimensions, but can be converted to two-dimensions by limiting the number of cells to unity in the irrelevant dimension. In this work the models were defined with a 1 meter thickness in the y-dimension.

blockMesh allows for the use of grading along the patches. This effect lets the cell-distribution to be skewed towards the region of interest. The cell expansion ratios was calculated in scripts based on the codes found on the OpenFOAM Wiki [1].

It is assumed that the shed vortices becomes easily turbulent. This implies that the mesh resolution is chosen in a way to disregard small scale vortices, and the numeric dissipation mimics

---

[1]Webpage accessed 08.06.2015 `http://openfoamwiki.net/index.php/Scripts/blockMesh_grading_calculation`

the turbulence dissipation. The work of Kristiansen and Faltinsen (2008) also shows that boundary layer on the inflow can be neglected. These assumptions enables the use of a laminar model for the flow, rather then a more complex turbulence model.

7.2 Numerical Set-Up - Towing Tank

7.2.1 Domain

The domain consists of a two-dimensional hull that is equipped with a moonpool. Since the boundary layer can be neglected the model can be simplified by not including the bow or the stern.
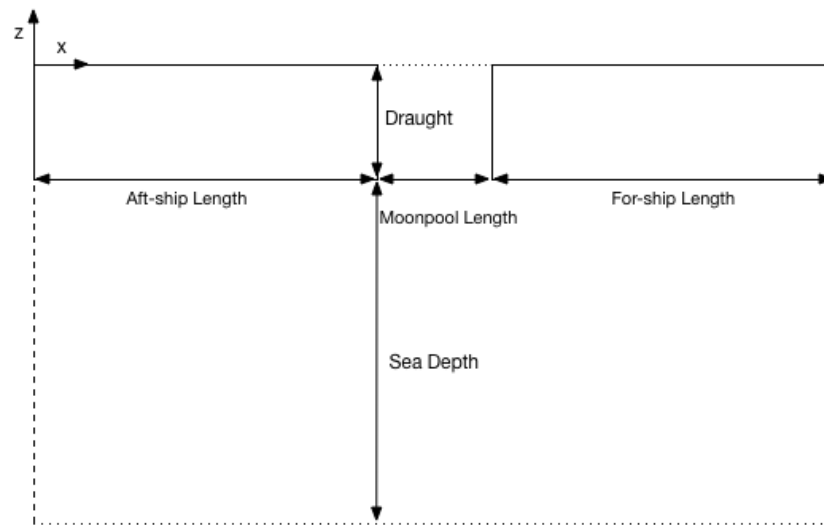

Figure 7.2: Illustration of the computational domain for the towing tank

The domain is illustrated in Figure 7.2, and we note that the origin is placed in the upper left corner. Thus the mean water-level is at $z = 0$ in accordance with recommendation from the developers of PVC3D. The figure illustrates the five unique length attributes that describes the case.

7.2.2 Boundary and Initial Conditions

The name of the different patches is illustrated in Figure 7.3 and the boundary and initial conditions for each patch is listed in Table 7.1. The table lists the boundary conditions as they are defined in the OpenFOAM environment. The following three flow parameters are defined for each patch; static pressure P, dynamic pressure $P - gh$ and the velocity U.
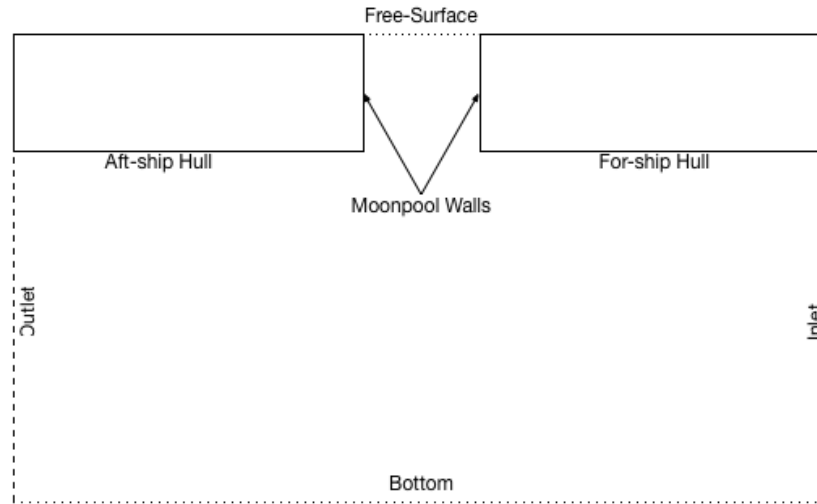
Figure 7.3: Illustration of the boundary conditions definitions for the towing tank.

Name	P	$P - gh$	U
Inlet	calculated (0)	fixedValue 0	pressureInletOutletVelocity (0 0 0)
Outlet	calculated (0)	zeroGradient	pressureInletOutletVelocity (0 0 0)
Bottom	calculated (0)	zeroGradient	slip
Hull	calculated (0)	zeroGradient	fixedValue (0 0 0)
Moonpool Walls	calculated (0)	zeroGradient	fixedValue (0 0 0)
Free Surface	calculated (0)	waveCurrentSurfacePressure	pressureInletOutletParSlipVelocity (0 0 0)
front, back	empty	emtpy	empty

Table 7.1: Table of the boundary and initial conditions for the towing tank.

The inlet is placed and the right-hand side of the domain, and the reference pressure is defined here as zero. The velocity at the inlet and outlet is defined from the pressure, and at the walls the no-slip condition is applied. The Free-Surface has the linear free-surface condition as explained in Section 6.2.5. Finally we assume that the bottom is far enough from the hull that the slip condition can be applied.

7.2.3   Mesh

In order to create a mesh for this problem, the domain was divided into four sub-blocks, as shown in Figure 7.4. The area in the vicinity of the moonpool opening has the most dense populations of cells, while the density diminishes further away from the opening.

Inside of the block that is situated within the moonpool, all the cells are squares. To insure stability at the corners of the moonpool, also the cells that are intercepting between the blocks are squares. However as the distance from the moonpool is increase, the cells stretches into larger rectangular shapes. This is illustrated in figure 7.4 as the arrows indicates the densest part of each block. Figure 7.5 shows the resulting mesh and illustrates the latter points.
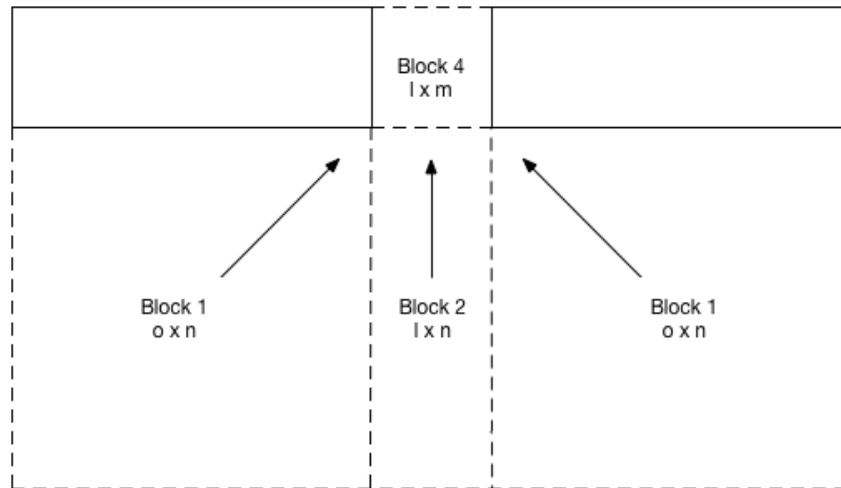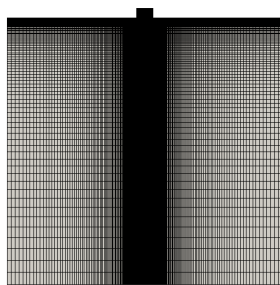
Figure 7.4: Illustration of the mesh strategy for the towing tank.

Figure 7.4 also illustrates the number of cells within each block. The primary parameter denotes the number of cells in the x-direction, and the second parameter in the y-direction. Due to the requirement of equal number of cells for each block in a intersection, the number of parameters the controls the number of cells are reduced to only four.

The number of cells required in our case will be investigated in the convergence section that follow in the next chapter.

(a) Picture of the whole mesh
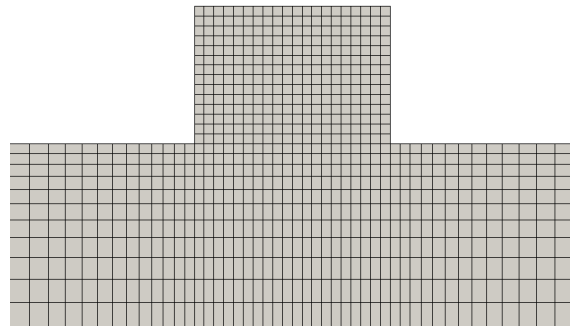
(b) Close up at the moonpool opening

Figure 7.5: Illustration of the final mesh for the towing tank.

7.2.4 Velocities & Time

In order to introduce the flow below the moonpool, a moving coordinate system was used. The velocity was linearly increased from zero to a desired velocity over 25 seconds.

The time step ΔT was chosen to be lowest values or the following two criteria; CFL equal to 0.5 or a 100th of a period of the expected oscillation.

7.3   Numerical Set-Up - Forced Heave

For reasons that will be discussed better later, it was necessary to create a secondary model, in order to estimate the natural periods of the moonpool. This model was inspired by the tutorial *incompressible/potentialFreeSurfaceFoam/oscillatingBox* included in OpenFOAM v2.1.0.

7.3.1   Domain

The main objective is to estimate the natural period for a moonpool, without forward speed or current present. Since the problem reduces to a radiation problem, symmetry can be utilised. As Figure 7.6 shows, the plane of symmetry goes through the centreline of the moonpool and only one half-hull is necessary to be included. It is important that the length of the tank is sufficient to give the radiated waves time to die out, before reaching the end of the tank.
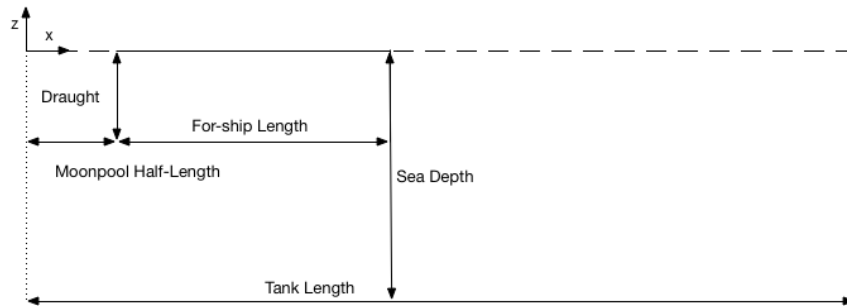

Figure 7.6: Illustration of the computational domain for the forced heave.

The final domain was 20 meters long and 2 meters deep, the half-moonpool measured 0.128 meters and the half-hull 1.972 meters. The draft of the hull was altered within a range of values to investigate.

7.3.2   Boundary and Initial Conditions

Figure 7.7 and the corresponding Table 7.2 shows the boundary conditions for this case. The conditions are similar to the previous Towing Tank set-up. Please note the symmetry boundary on the left-hand side. Since the hull is to oscillate only in the vertical direction, the boundary condition on the free-surface is simplified, ref Equation 6.8.

7.3.3   Mesh

The mesh was generated by *blockMesh*, but in contrast to the towing tank, only one block will be utilised with in domain. The resulting mesh is illustrated in figure 7.8, and as the figure shows,
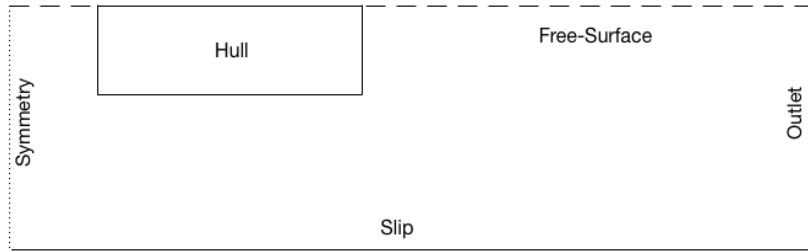
Figure 7.7: Illustration of the computational domain for the forced heave.

Name	P	$P - gh$	U
Symmetry	calculated (0)	zeroGradient	fixedValue (0 0 0)
Outlet	calculated (0)	zeroGradient	pressureInletOutletVelocity (0 0 0)
Hull	calculated (0)	zeroGradient	fixedValue (0 0 0)
Free Surface	calculated (0)	waveSurfacePressure	pressureInletOutletParSlipVelocity (0 0 0)
Bottom	calculated (0)	zeroGradient	slip
front, back	empty	emtpy	empty

Table 7.2: Table of the boundary and initial conditions for the forced heave.

the block has the highest density within the moonpool in the upper left corner, and the distrobution of cells stretches out as we move away from the moonpool. The hull it self was implemented with the OpenFOAM tools *topoSet* and *subsetMesh*, which in short removes the computational cells with the hull and applies the hull boundary condition in the new border.
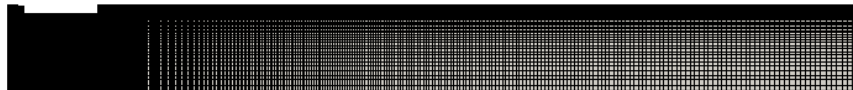

Figure 7.8: Illustration of the resulting mesh for the forced heave.

The mesh consists of 400 cells in the horizontal direction and 40 cells in vertically. Within the moonpool the resulting grid was 10 times 7 cells.

7.3.4 Velocities & Time

The flow velocities are set at zero and the system is initially at rest as the simulations is started. However the velocity boundary condition for the hull, is free to oscillate. The oscillation was 0.01 meter and for each case the period of oscillation was altered to investigate the response. In each simulation the oscillation starts with a amplitude of zero, and the amplitude develops linearly over 10 periods of oscillation. The total simulation time was 40 periods, and the final value was extracted as the mean response of the last 20 periods of oscillation.

The time step ΔT was chosen to be lowest values or the following two criteria; CFL equal to 0.5 or a 100th of a period of the expected oscillation.

7.4   Simulation Environment

The simulation was conducted on a personal MacBook Pro 13" with 8GB RAM and a 2,6 GHz Intel i5 processor. The simulations was conducted utilising a virtual machine with Ubuntu v. 15.04 and OpenFOAM v. 2.3.0. installed. The PVC3D package was installed on-top of this with guidance of MARINTEK. Post-processing was conducted using ParaView and TecPlot 360, and the languages MATLAB, GNU Octave and GNU m4 was utilised to execute a range of scripts in both pre- and post-processing.

The philosophy of all work was to develop simple template cases that was controlled by a list of parameters. Normally these parameters are spread across a number of places within the case-dictionary, however simple scripts was created in order to generate cases from a simple spreadsheet of variables.

Chapter 8

Results and Discussion

8.1 Introduction

In this chapter we will present the results from the conducted simulation campaign. Discussions will be made underway as the results are presented.

8.2 Forced Heave

For any oscillation motion the natural frequency is a parameter of great importance. In order to estimate this frequency for our problem, the hull will be introduced to a forced heave oscillation. By altering the the frequency of oscillation, it is expected that the water column in the moonpool will start to oscillate as well. The natural frequency is then estimated to be the one oscillation frequency that produces the highest resonance amplitude. These test are conducted without any forward velocities or other disturbances.

The forced heave tests were first attempted on the same models as the towing tank models. This model did however prove to be problematic, with regards of the stability of the solver. It is assumed that the lack of an outer free-surface, creates a limiting and unphysical model. Technically the trend for the resulting moonpool oscillation decreased exponentially negatively, and even extracting data from the first oscillation proved itself extremely difficult.

Inspired by a tutorial that is included in the openFOAM package and earlier works on gap resonance by Kristiansen and Faltinsen (2012), a new model was created, as detailed in Section 7.3.

8.2.1 Results

The model was set up as described in Section 7.3.1 a total moonpool length of 0.256 meter and a half-hull of 1.972 meter. The following three draft-to-length ratios was investigated; $d/l =$ [0.6, 0.7, 0.8]. The oscillations on the hull was modelled as a sinusoidal function, and the amplitude was linearly increased from zero to a final value of 0.01 m over 10 periods. Each case ran for a total of 40 periods, and the mean of the last 20 periods was used as the measurement value. A case is illustrated in Figure 8.1, where the red line represents the oscillations of the hull, the blue line is the mean oscillation of the free-surface, and finally the peaks that are marked with a yellow stars is the ones used in the measurement.
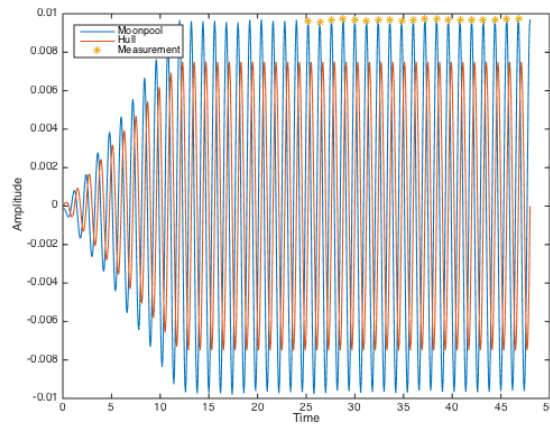

Figure 8.1: Sample oscilllation results for a case of the forced heave.

The results are presentment graphically in Figure 8.2, where the circles represents each frequency that was simulated, and the line is curve-fitted. The natural frequencies are also represented in Table 8.1, were they are compared to numerical estimations from Molin (2001) for a 2D moonpool, Equation 4.6. The numerical beam length were conservatively assumed to be equal to the actual beam, i.e. $B_T = 1.0B$. The estimations from Molin underestimates the natural period, but this is also observed by Fredriksen (2015). Since the benchmark case is a three-dimensional model, it is not possible to compare this data with the numerical findings.

d/l	Molin (2001) $T_0[sec]$	Simulation $T_0[sec]$
0,6	1,25	1,44
0,7	1,29	1,51
0,8	1,33	1,54

Table 8.1: Comparison of the Natural Periods in heave for a 2D moonpool, l = 0.256 m
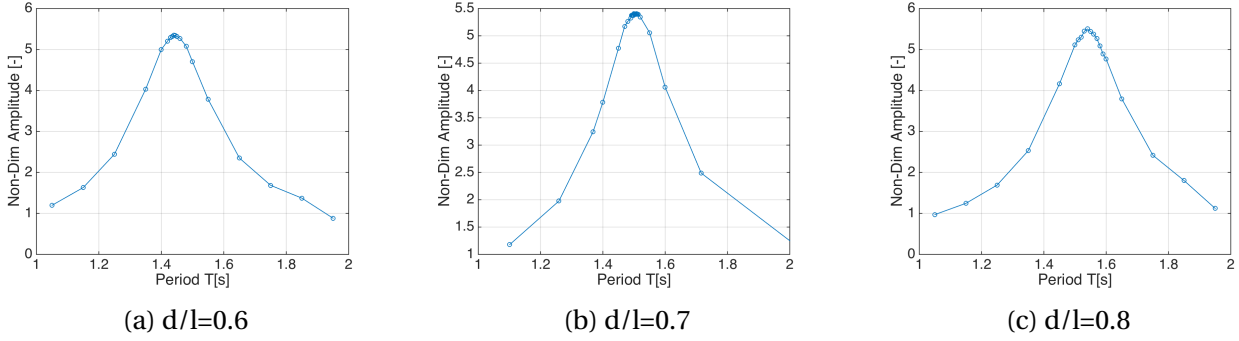
Figure 8.2: Non-dimmensional heave amplitudes for different drafts.

The results from this numerical investigations demonstrates an expected trend. The natural periods increases as the draft becomes larger.

8.3   Towing Test

The towing tests were the main objective of this simulation campaign, and the goals were to replicate the reported piston-mode development for a moonpool at different speeds. In order to verify this work, the results were compared to measurements data as reported by van 't Veer and Tholen (2008). In the paper there some key issues that are not commented on, thus several aspects of this simulations are untouched territory. Several observations made during this work will be presented in this section.

8.3.1   Moonpool Scaling

In the existing literature, many of the results are presented by mean of the reduced velocity, $U' = U/(\omega_0 l)$. This parameter is dependent on the natural frequency and the length of the moonpool, but it is not necessarily easy to see how this parameter scales with regards to the velocities.

To evaluate this problem, we seek the relationship between the velocity in full scale and model scale. We need to relate these velocities to the scale factor $\lambda = L_F/L_M$. By expressing the natural frequency in the model scal as the formulations of DNV (2011) as in Equation 4.5, the relationship can been evaluated by inserting for the parameters in full scale.

$$U'_M = \frac{U_M}{(\omega_0 l)_M} = \frac{U_M}{\left(\sqrt{\frac{g}{\lambda^{-1}d + \kappa\sqrt{\lambda^{-2}S}}}\right)(\lambda^{-1}l)} = \frac{U_M}{(\omega_0 l)_F \lambda^{-1/2}} \tag{8.1}$$

Equation 8.1 reviles that given a Froude scaling of the velocity, $U_F = U_M\lambda^{1/2}$, the reduced velocity scales in the similar manner.

8.3.2   Development of Oscillation Amplitude

Time-Series

During the literature study it was not reviled any material that presents a longer time-series for the piston-mode amplitude. The initial guess was that the oscillations would build up over time, before reaching a stable maximum value. However the results from the simulations shows that the system is, in one sense, more unstable then expected.

The results from a example case is shown in Figure 8.4a, were the oscillation amplitude is plotted in blue, and the peaks are highlighted by a red line. This figure shows that the oscillation reaches a maximum value, before its trend seem to be negative towards a lower stable value.

The development illustrates how we can use a control system analogy for the moonpool problem. The oscillation is driven by the vortex creation at the leading edge, which in turn is a function of the velocity regime in this area. As the water column starts to oscillate, it will induce new velocities at the leading edge, which in turn interacts with the vortices. A flowchart for this analogy is shown in figure 8.3.
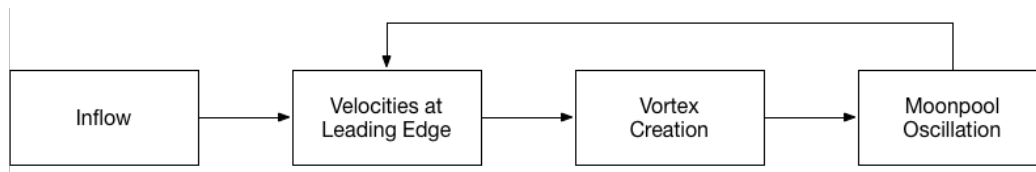

Figure 8.3: Control system analogy

(a) Case Amplitude Example

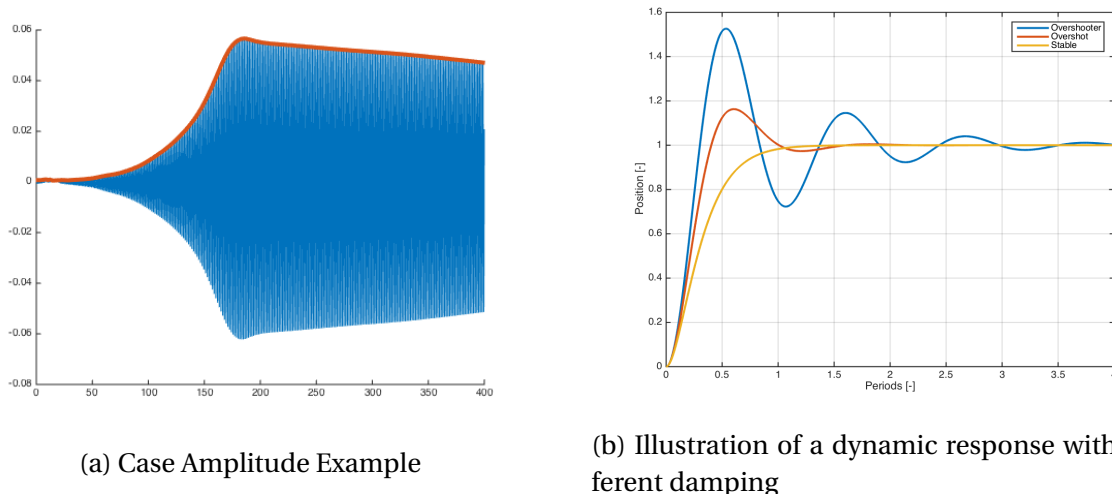(b) Illustration of a dynamic response with different damping

Figure 8.4: Step response analogy for the development of oscillation amplitude.

This analogy can further be used to exemplify the stability of the system. In Figure 8.4b, we see the development of a dynamic system with different levels of damping. In the world of con-

troller systems this resemblances a step response. The figure shows how the system stability is of importance for the development of the response. It is possible to argue for a similar development for the moonpool amplitude. Depending of the systems total stability, the amplitude will behave in different manner over time.

Flow Characteristics

The flow in the moonpool during oscillation is visualised in Appendix B. The total and dynamic pressure, velocity and vorticity is plotted at four distinct time-steps during a single oscillation. The results compare well with the expectations, and in side-by-side comparison with pictures from Fukuda (1977). These pictures are also included in Appendix B.

8.3.3   Method of Measurement

We have previously discussed the methods of measurements that were used in the benchmark experiments. We seek to quantify the mean of the amplitude, based on a time-sample that starts around the visual maximum and lasts over 60 oscillations. As proven earlier the natural period for main model (d/l=0.7) was 1.51 seconds. In order to sample over 60 oscillation the time-window becomes 90 seconds. Due to the usage of *observed maximum amplitude*, the time-window is extracted further 10 seconds backwards for good measures.

   The amplitude of each time-step is evaluated as the mean of the elevation for all cells on the free-surface. In the reference experiment the amplitude was measured from three individual wave-height sensors along the moonpool length.

   In Figure B.1 we can see how all this is implemented in for a single case. The black vertical lines marks the limits of the time-window, which spans over 100 seconds. The red dotted line marks the limit of the towing tank in the reference experiment, while the solid red line is the limits of a extended tank that assures similarity in the number of oscillations.
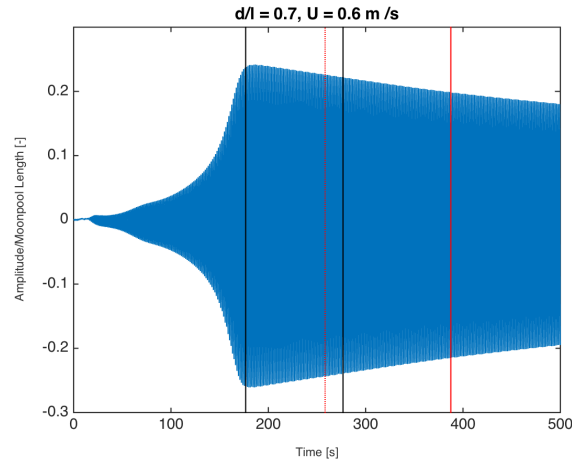
Figure 8.5: Illustrations of the measurement of the data from an example case.

8.3.4   Convergence Study

The goals of an convergence test is to verify and optimise the mesh, the domain and the time-step for a simulation. By verification it is implied that the results stabilises as the parameters are refined. Optimisation on the other hand seeks to find the the most effective parameters in terms of computational time.

In this campaign the end-result for each run is the mean of the observed amplitude over a time-window. Of this reason, this single value, is sufficient to be investigated in the convergence test.

As a conservative estimate we defined the domain to be equal in length to the model in the experiments, L = 4.2 m. The depth of the domain was set to 1,5 L. The moonpool length equals 0.256 m. and the draft of the model was 0.1792 m., i.e. $d/l = 0.7$.

For simplicity the mesh tactic was defined by only two parameters **l** - **n**, see Figure 7.4, where **l**, is the number of cells along the length of the moonpool, and **n** is the number of cell both along the half-hulls and the depths of the domain. The last parameter **m** was calculated to create square cells with in the moonpool.

The mesh convergence test is shown in Figures 8.6a and 8.6a for two different velocities. The figures shows that the amplitude increases as the grid becomes more dense. From these figures we can conclude that the 60-90 mesh is sufficient for this geometry.

(a) Mesh Convergence
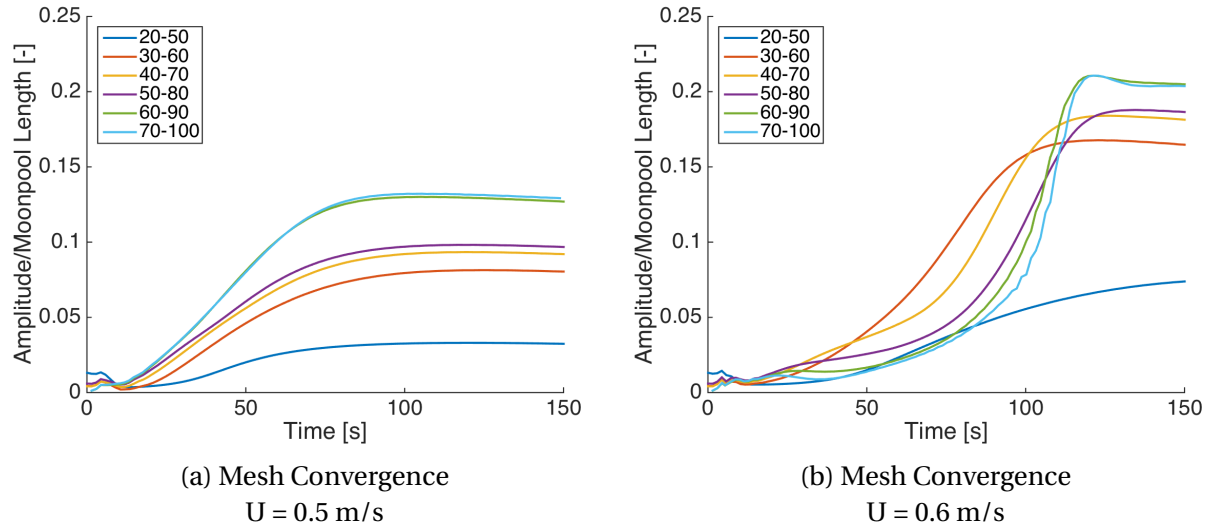U = 0.5 m/s

(b) Mesh Convergence
U = 0.6 m/s

Figure 8.6: Graphical presentation from the mesh convergence

Now that we have convergence for our conservative and large domain, the next is to perform a convergence test on the domain itself. This is primarily to confirm that the domain is not too small, which can cause the boundaries to interfere numerically with the solution. In Figure 8.7a and the complementing Table 8.2, it is illustrated how the amplitude development changed for different domains. The domain was either extracted with additional blocks, or cells was deleted from the domain to reduce a length. This preserved a equal distribution of the cells, and consistency in the results.

Case	Domain			Non-Dimentional	
	Length	Depth	# Cells	Max Amplitude	Sample
1	1,0 L	1,5 L	24066	0,21064	0,21064
2	1,0 L	1,0 L	21897	0,21057	0,21067
3	1,0 L	0,75 L	20451	0,21081	0,21081
4	2,0 L	1,5 L	26978	0,21536	0,21360
5	3,0 L	1,5 L	29890	0,22159	0,22146

Table 8.2: Resulting results from the domain analysis

The results from the domain analysis shows that a reduction of the depth mainly shifts the amplitude development on the time scale. Interestingly a longer domain gives a fractional increase in the amplitude, but in this analysis we will regard that contribution to be neglect-able. The final domain was set to be quadratic with lengths L, and a mesh $60 - 90$ by the conventions explained earlier.
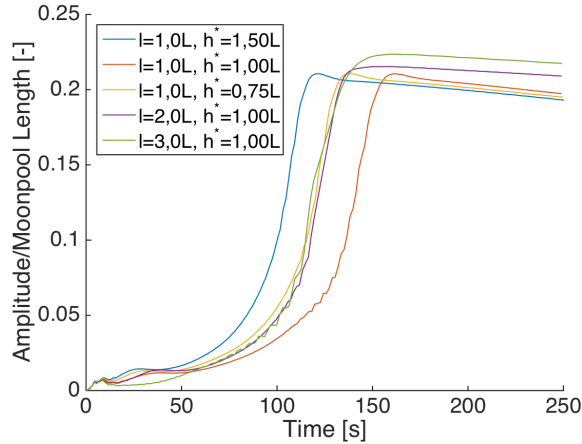
(a) Domain Convergence
Mesh 60-90, U = 0.6 m/s

Figure 8.7: Graphical presentation from the domain convergence.

8.3.5   Piston Mode Development

The primary goal of this simulation campaign was to recreate the piston-mode amplitude development, as reported in van 't Veer and Tholen (2008). The results from this work and the reference experiment is presented in Figure 8.8. The time-series that forms the basis for each data-point is presented in Appendix C.1 and C.2.

It can be seen that the onset velocity is identical, while the linear slope is higher for the simulations then for the experiments.

Recalling the formulations of Fukuda (1977) in Equation 4.12, the expected slope for a clean moonpool were $3\pi/16 \approx 0.589$, given $b_2 = 1/2$. In the experiments the slope is in the order ≈ 1, which is a value that is 70% higher. Equation 4.12 is derived from the equations of motion for a three-dimensional problem, thus is also the current quadratic damping coefficient b_2 derived in the same numbers of dimension.

We do not hold a expression for the quadratic damping for a two-dimensional model, Given that the constant term in the Equation 4.12 is fixed, the slope from the simulation would require a quadratic damping term of $b_2 = 3\pi/32 \approx 0.294$.

A higher slope in two-dimension is to be expected due to the lack of three-dimensional effect. We will come back to this topic in Section 8.4.

The so-called offset velocity, where the oscillations vanishes, proved to be difficult to define. As illustrated in Figure 8.9, the oscillation takes a longer time to build up as the velocity of the hull increases. For case where the velocity is 0.75 m/s, we can see that the build-up happens just after the end of the towing tank.
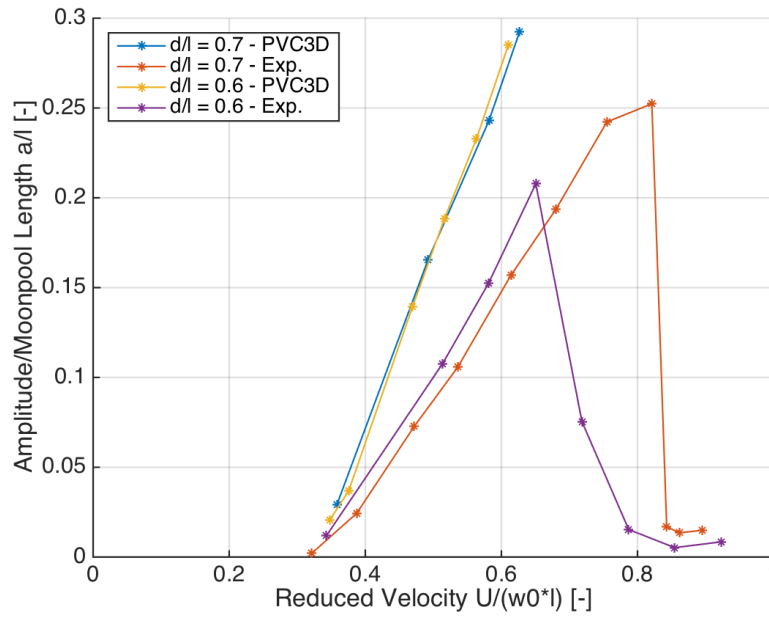
Figure 8.8: Piston-mode amplitude development due to forward velocities

It can be speculated in that the two-dimensional and laminar model, is too idealised and symmetrical. By that we mean that the vortex shedding is most likely driven by disturbances, and that these needs unphysical amount of time to build up in our simulations.
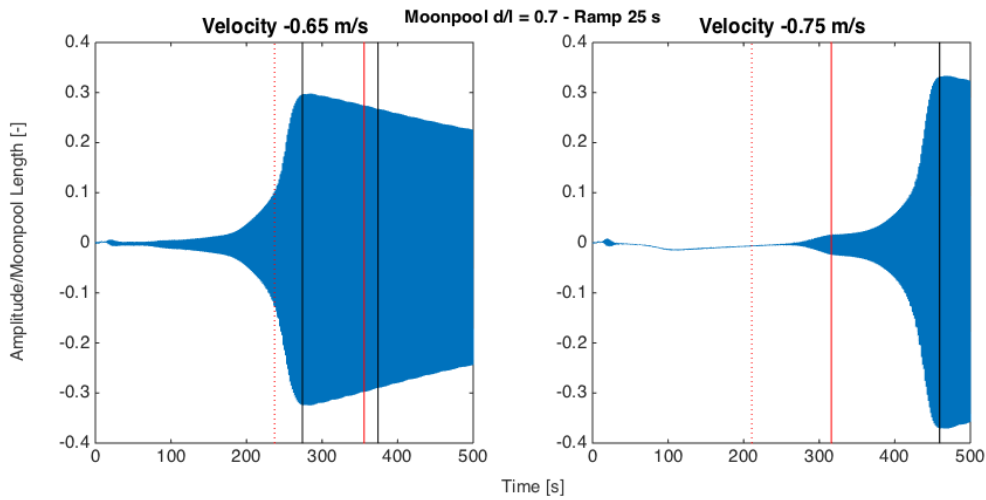

Figure 8.9: Example results highlighting the onset and offset Time.

8.3.6   Resistance on the Hull

The resistance on the hull can be quantified by integrating the pressure that are acting on the inner moonpool walls. Due to the linearised boundary condition on the free-surface, this needs to be handled with special care, as illustrated in Figure 8.10.
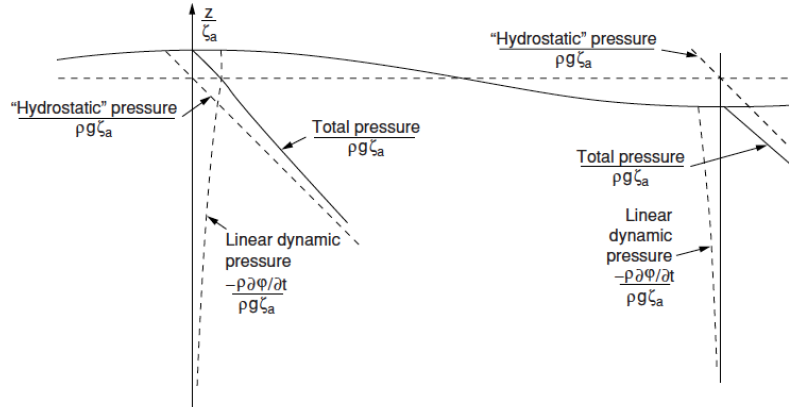
Figure 8.10: Pressure variation under a wave crest and a wave trough according to linear wave theory, Faltinsen (2006).

Mathematically this can evaluated with the following two integral.

$$F_{2D} = \int_{-d}^{z=h} P(z)\,dz \qquad\qquad\qquad h < 0 \qquad\qquad (8.2)$$

$$F_{2D} = \int_{-d}^{z=0} P(z)\,dz + \frac{1}{2}P(0)\,h \qquad\qquad h > 0 \qquad\qquad (8.3)$$

Where $P(z)$ is the total pressure, d is the draft of the moonpool and h is the surface elevation within the moonpool. In our numerical analysis this can easily be implemented by setting dz equal to the height of each cell, and the expressions reduces to a sum of all cells on the vertical wall.

The sum of the forces acting on the moonpool walls are plotted in Figure 8.11b. Positive direction is defined in the positive x-axis, thus a negative force equals a resistance on the hull. By comparison with the mean free-surface that is shown in Figure 8.11a, we can see that the oscillation causes a resistance on the hull as the oscillation moves from the equilibrium level and up to its peak. Similarly the hull seem to get a push as the oscillation reduces from the peak level, down to equilibrium. As long as the free-surface has a negative value, there are presumingly no forces acting on the moonpool walls.

The negative part of the total force resembles the expected shape as from the linear momentum theory as presented in Section 5.3. However from comparison with Figure 8.11d, we see that the magnitudes of the forces are not in the same order.

Visual exception of the free-surface shows that there is always some sloshing movement inside of the moonpool. This causes a asymmetrical water-level on the walls, and thus a difference in the statical pressure. By defining $\hat{h}$ as the difference between the water level on the upstream and downstream wall, the asymmetrical part of the statical presure can be expressed by the following expression.

$$F_{2D} = 2\rho g d \hat{h} \tag{8.4}$$

Where ρ is the density of the water, g the gravitational acceleration and d the draft of the moonpool.

In Figure 8.11c we can see how the statical pressure develops over one period, and some observations can be made. The force-contribution is non-zero when as the free-surface is negative. Since the total is zero in this area, there has to be contribution and neutralising contribution in the dynamic pressure. In the range where the free-surface is positive, the sloshing forces seem to align with the total force, but not in the magnitude of the forces.

The time average of the total force can be expressed as the moonpool resistance coefficient, see Equation 5.1. This value was computed all the individual simulations as presented in Appendices C.2 and C.1. The values of C_{MP} ranged from 0.25 to 0.77, which is much higher then those reported in the literature, see Figure 3.6. A scatterplot of our results are included in Appendix E.
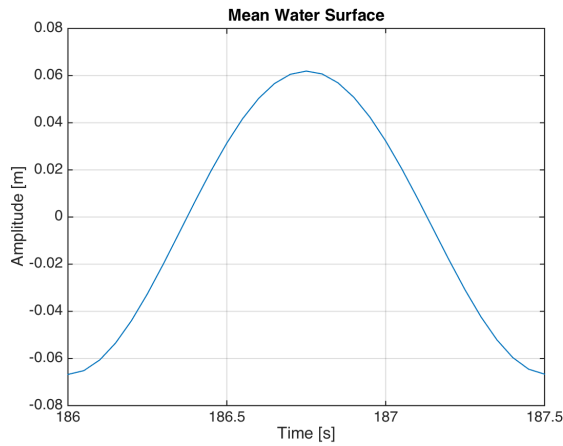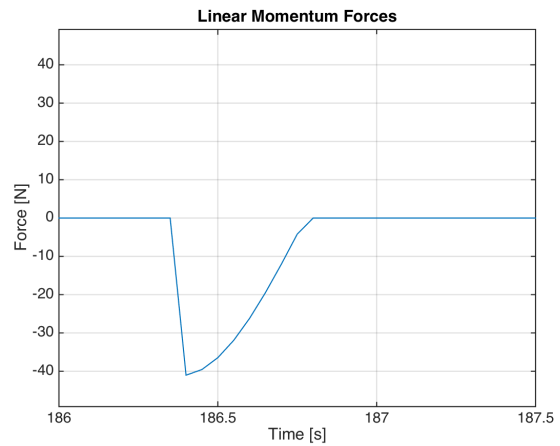
(a) Mean Water Elevation.
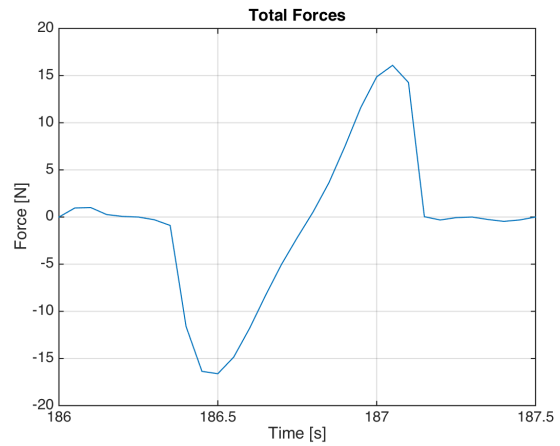
(b) Total Forces acting on the Hull in x-direction.
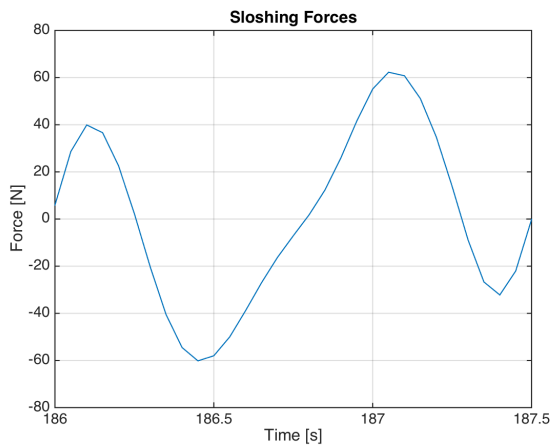
(c) Statical Force Difference due to Sloshing.

(d) Theoretical Force from Linear Momentum, ref Section 5.3.

Figure 8.11: Graphical presentation of the forces in a moonpool during one period.

8.4 Discussion

8.4.1 Three Dimensional Effects

The results from the numerical two-dimensional tests reviled that the amplitudes of the piston-mode oscillation was slighly higher then in the three-dimensional experiments. This fact can be explained by arguments around the idealisation of a moonpool as a two-dimensional slice.

The first argument to consider, is that the the vortex distribution after a step is not uniform. As illustrated in Figure 8.12a, 3D-effects from the sidewalls leads to the fact that the vortex distribution is strongest along the centreline in the moonpool. The 2D model can be said to replicate the centreline due to the lack of sidewalls, hence being exposed to the strongest vortices.

The non-uniform vortex distribution in the moonpool would potential lead to connected non-uniform amplitude in the cross-section normal to the flow direction. This is highlighted in Figure 8.12b, were we see that as the centreline is elevated, water will flow out to the sidewalls were the elevation is lower.

(a) Vortex distribution over a step.

(b) A oscillating 2D slice.
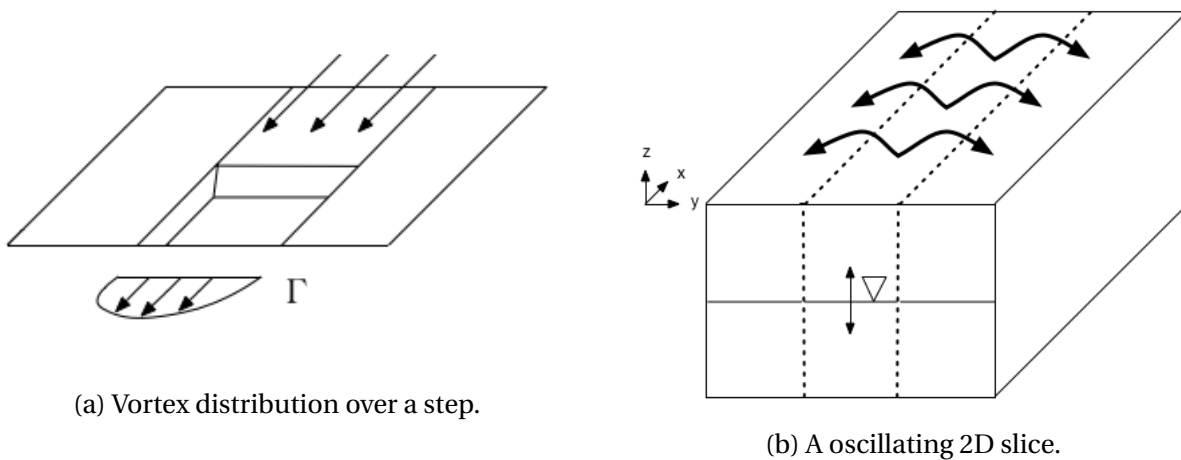
Figure 8.12: Illustrations of physical aspects that plays a role in the two- versus three-dimensional argument.

8.4.2 Offset Velocity

The results for different velocities shows that the oscillations takes time to build up. Figure 8.9 shows that in a high velocities the oscillation is not started before the end of the towing tank. As mentioned, it is possible that the two-dimensional model is to idealised and that different results might have been achieved by the introduction of distortions in the velocity field.

Due to the lack of a time-series from experimental data, it is not necessarily simple to say if the same trend will be seen in a real moonpool. The flow regime beneath a hull will be turbulent and the most likely reduce the time required before the oscillations starts. On the other hand,

by using the tank length as a limiting factor, the results from the simulations are similar to the experiments.

8.5   Results Applied on a Offshore Vessel

Until now, we have only used the reduced velocities in order to express the amplitude development. For the sake of discussion we will now insert the physical values that represents a typical moonpool on a offshore vessel. Recalling the mean values from the DOF fleet in Section 1.6, a typical moonpool has the dimensions 7,2x7,2 meters at the keel and 9.2x9.2 meters at the deck. The draft of the hull is 7,4 meters and the expansion of the moonpool happens at 0,8 meters above the keel. This geometry will have a natural period of 7,52 seconds by the formulations of DNV (2011) in Equation 4.5. By inserting these parameters in the Figure 8.8, the following figure can be produced.
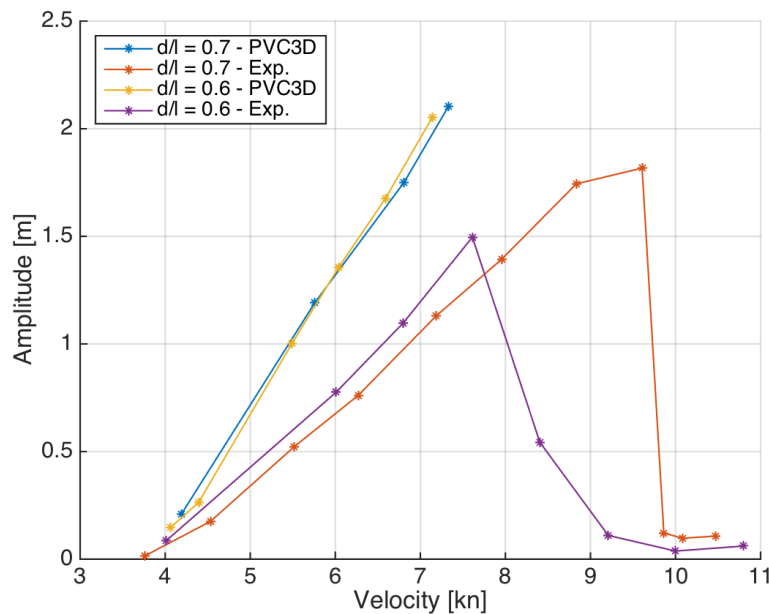
Figure 8.13: Piston-mode amplitude development due to forward velocities on a offshore vessel

As we can see from this figure the piston-mode is expected become observable at 4 knots, and a maximum amplitude of 1,5 meters around 8 knots. The oscillations are expected to vanish in velocities that are over 9 knots. Most offshore vessels have a operation operational speed in the range of 12 - 15 knots, it is therefore likely that the piston-mode phenomena can be neglected for all practical appliances.

In Section 5.3 a review of the resistance of the hull as a function of the oscillation amplitude

was given. Expressed by the dimensional-less C_{MP}, the resistance peaks at values in the magnitude of 0.1, see Figure 5.1. In order to express this coefficient in dimensional units, we will utilise the data from the towing test conducted in Kristiansen (2006). The model has a square moonpool with the dimensions of 0.3573 x 0.3573 meters, or 7.2 x 7.2 in full scale. The added resistance on the hull, given a coefficient of 0.1, is illustrated in Table 8.3.

Velocity Full-Scale	Velocity Model-Scale	Red. Velocity -	Resistance Hull	Added Resistance Piston-Mode	Percentage Increase
$[kn]$	$[m/s]$	$[-]$	$[N]$	$[N]$	$[-]$
12	1.37	0.82	30.75	11.99	39 %
14	1.60	0.96	42.93	16.40	38 %
16	1.83	1.09	50.77	21.41	42 %
18	2.05	1.23	71.31	27.04	38 %

Table 8.3: Added resistance coefficient $C_{MP} = 0.1$, applied on the experiments from Kristiansen (2006)

In the towing tests on that was conducted on this model, the velocities were higher then range where piston-mode is expected. Even though, the results in Table 8.3 shows how the relative added resistance as a percentage, for several velocities. Surprisingly, the trend relieves that given a $C_{MP} = 0.1$, the resistance on a offshore vessel might increase in a magnitude of 40 %. Please note that this number is for the total contribution, i.e. base resistance and the oscillation resistance. The base resistance for this model was found to be 6 %.

Part IV

Concluding Remarks

Chapter 9

Conclusion

This work has shown that the added resistance due to the moonpool, will have a considerable contribution on the hull of a offshore vessels. A constant resistance is expected to be in the range of 5 - 10 %, and is dependent on the placement of moonpool and the general flow regime beneath the hull.

Simulations were conducted to replicate and verify the expected development of the vertical piston-mode oscillation. Even though the model was simplified to a two-dimensional case, the results were promising and verified that the piston-mode is expected to be observed over a limited velocity range. For an offshore vessel the latter velocity range in calm waters are below the normal service speeds. This means that the oscillations will be avoided in the common operational modes for the vessels.

However, if the velocity is reduced due some arbitrary influence, it is still interesting to quantify the resistance associated with the oscillation. This can be achieved by utilising the formulations by Fukuda (1977), as given in Equations 4.12 and 5.4. These needs to be complimented with the natural frequency as given by DNV (2011) in Equation 4.5, and a velocity range of $U' = \frac{U}{\omega_0 l} \in [0.35 - 0.80]$, where the outer limits represent the onset and offset velocity. This was exemplified in details for a sample vessel in Section 8.5. On the basis of the existing literature, it was shown that the oscillations in calm water might further increase the resistance on the hull, by a factor of 30 %.

Several aspects of this study are related to uncertainties and the lack of published literature in direct relation to offshore vessels.

Chapter 10

Further Work

During the work of this thesis it was quickly reviled how complex the physics behind the problem can be. Several aspects needs to be highlighted as these topics deserve more attention.

Moonpool Modelling - The excitation force for the piston-mode for a moonpool on a vessel with forward speeds is not well established. We concluded that this is related to the vortex shedding on the leading edge of the moonpool, hence it should be possible to describe this shedding in terms of its frequency.

The natural frequencies used in this work was established at zero forward velocity. It is however expected that these frequencies will be altered in the situation with forward velocities.

CFD - Simulation Campaigns - The simulations that were conducted in this work was only benchmarked against some data-points extracted from figures in older literature. This is far for a ideal situation, and is recommended to conduct experiments to confirm several aspects of the simulations.

Waves - This work focused on the calm water conditions. To describe the phenomena in more realistically scenarios, it is necessarily to perform a study in waves.

Bibliography

Aalbers, A. (1984). The water motions in a moonpool. *Ocean engineering*, 11(6).

Berget, K., Sauder, T., and Skejic, R. (2009). Water Dynamics in a moonpool - Litterature Study. Technical report, MARINTEK.

Çengel, Y. A. and Cimbala, J. M. (2015). *Fluid Mechanics - Fundamentals and Applications*. McGrawHil, 2.ed. edition.

Choi, Y.-b. (2014). Device for diminishing flow resistance in moon pool.

Cotteleer, A. (2000). *Experimental study on water motions in a moonpool caused by forward speed of the ship*. Master thesis, Delft.

DeepOcean (2008). Edda Fauna - Vessel Specification Sheet.

DNV (2011). Modelling and Analysis of Marine Operations. Technical Report APRIL 2011.

DOF Group ASA (2014). *2014 - The DOF Fleet*.

Dommermuth, D. G. and Yue, D. K. P. (1987). Numerical simulations of nonlinear axisymmetric flows with a free surface. *Journal of Fluid Mechanics*, 178(-1):195.

English, J. (1976). A means of reducing the oscillations in drillwells caused by vessels' forward speed. (May):69–70.

Faltinsen, O. (1993). *Sea Loads on Ships and Offshore Structures*. Cambridge Ocean Technology Series. Cambridge University Press.

Faltinsen, O. M. (2006). *Hydrodynamics of High-Speed Marine Vehicles*. Cambridge University Press.

Faltinsen, O. M. and Timokha, A. N. (2009). *Sloshing*. Cambridge University Press.

Ferziger, J. H. and Peric, M. (2001). *Computational Methods for Fluid Dynamics*. Springer Berlin Heidelberg.

Fredriksen, A. G. (2015). *A numerical and experimental study of a two-dimensional body with moonpool in waves and current.* PhD thesis, NTNU.

Fredriksen, A. G., Kristiansen, T., and Faltinsen, O. M. (2014). Experimental and numerical investigation of wave resonance in moonpools at low forward speed. *Applied Ocean Research*, 47:28–46.

Fukuda, K. (1977). Behavior of Water in Vertical Well with Bottom Opening of Ship, and its Effects on Ship-Motion.

Fukuda, K. and Yoshii, Y. (2009). Flow Calculation in Vertical Cavity with Free Surface and Bottom Opening to Water Stream. *Journal of the Japan Society of Naval Architects and Ocean Engineers*, 10(6):23–28.

Gaillarde, G. and Cotteleer, A. (2001). Water motion in moonpools empirical and theoretical approach. *Maritime Research Institute Netherlands MARIN*.

Hammargren, E. and Törnblom, J. (2012). *Effect of the Moonpool on the Total Resistance of a Drillship.* Master thesis, Chalmers University of Technology.

Knott, G. F. and Mackley, M. R. (1980). On Eddy motions near plates and ducts, induced by water waves and periodic flows. *Philosophical Transactions of the Royal Society of London. Series A. Mathematical and Physical Sciences*, 294(1412):599–623.

Kristiansen, A. S. (2006). *Measures to reduce resistance on an open moonpool.* Master thesis, NTNU.

Kristiansen, T. and Faltinsen, O. M. (2008). Application of a vortex tracking method to the piston-like behaviour in a semi-entrained vertical gap. *Applied Ocean Research*, 30(1):1–16.

Kristiansen, T. and Faltinsen, O. M. (2012). Gap resonance analyzed by a new domain-decomposition method combining potential and viscous flow DRAFT. *Applied Ocean Research*, 34:198–208.

Kristiansen, T., Sauder, T., and Firoozkoohi, R. (2013). Validation of a Hybrid Code Combining Potential and Viscous Flow With Application to 3D Moonpool. *ASME 2013 . . .*, pages 1–9.

Larsson Lars, R. H. C. (2010). *Ship Resistance and Flow.* Society of Naval Architects and Marine Engineers (SNAME).

Maisondieu, C. and Ferrant, P. (2003). Evaluation of the 3D Flow Dynamics in a Moonpool. *Proceedings of The Thirteenth (2003) International Offshore and Polar Engineering Conference*, 5:493–500.

Molin, B. (2001). On the piston and sloshing modes in moonpools. *Journal of Fluid Mechanics*, 430:27–50.

Naudascher, E. and Rockwell, D. (2012). *Flow-Induced Vibrations: An Engineering Guide.* Dover Civil and Mechanical Engineering. Dover Publications.

Rockwell, D., Lin, J.-C., Oshkai, P., Reiss, M., and Pollack, M. (2003). Shallow cavity flow tone experiments: onset of locked-on states. *Journal of Fluids and Structures*, 17(3):381–414.

Rockwell, D. and Naudascher, E. (1979). Self-Sustained Oscillations of Impinging Free Shear Layers. *Annual Review of Fluid Mechanics*, 11:67–94.

Sadiq, S. and Yao, X.-l. (2014). Combined Acoustic and Hydrodynamic Experimental Data. pages 1–9.

Spangeberg, S. r. and Jacobsen, B. K. (1983). Reduction of the water motion in the moonpool. *Marintec Offshore China Conference, Shanghai*, page 13.

Sverre Steen (2013). Lecture Notes in TMR4220 Naval Hydrodynamics Ship Resistance.

van 't Veer, R. and Tholen, H. J. (2008). Added Resistance of Moonpools in Calm Water. *Volume 6: Nick Newman Symposium on Marine Hydrodynamics; Yoshida and Maeda Special Symposium on Ocean Space Utilization; Special Symposium on Offshore Renewable Energy*, pages 153–162.

Zoccola, P. J. and Farabee, T. M. (2001). On the frequency of sheartones. *Acoustics Research Letters Online*, 2(December 2000):13.

Part V

Appendixes

Appendix A

Extract of Vessels from the DOF Fleet

Vessel Data				Moonpool Geometry		
Vessel Name	LOA	B	D	L	B	S
-	*m*	*m*	*m*	*m*	*m*	*m*^{2}
Anchor Handling Tug Supply Vessels (AHTS)						
Skandi Vega	109,5	24,0	7,8	7,2	7,2	51,84
Construction Support Vessels (CSV)						
Skandi Acergy	156,9	27,0	8,5	7,2	7,2	51,84
Skandi Aker	156,9	27,0	8,5	7,2	7,2	51,84
Skandi Artic	156,9	27,0	8,5	7,25	7,25	52,56
Skandi Constructor	120,2	25,0	8,0	8,0	8,0	64,00
Geosea	84,8	15,0	5,0	5,5	6,0	33,00
Geosund	98,5	18,8	5,9	7,1	6,0	42,60
Skandi Hercules	109,5	24,0	7,8	7,2	7,2	51,84
Skandi Neptune	104,2	24,0	6,3	7,2	7,2	51,84
Skandi Niteroi	142,2	27,0	8,5	7,2	7,2	51,84
Ocean Protector	105,9	21,0	6,6	7,2	7,2	51,84
Skandi Salvador	105,9	21,0	6,6	7,2	7,2	51,84
Skandi Seven	120,7	23,0	7,0	7,2	7,2	51,84
Skandi Skansen	107,2	24,0	7,8	7,2	7,2	51,84
Skandi Skolten	109,5	24,0	7,8	7,2	7,2	51,84
Skandi Vitoria	142,2	27,0	8,5	7,2	7,2	51,84
Newbuilding (CSV)						
EP9	139,9	28,0	8,5	7,2	7,2	51,84
EP10	139,9	28,0	8,5	7,2	7,2	51,84
NB800	160,9	32,0	9,25	9,4	7,2	67,68
NB823	146,0	30,0	8,5	9,1	7,2	65,52
NB824	146,0	30,0	8,5	9,1	7,2	65,52

Table A.1: Table of the DOF vessels with working class moonpools (DOF Group ASA (2014)).

Appendix B

Visualisations of the Moonpool Oscillation
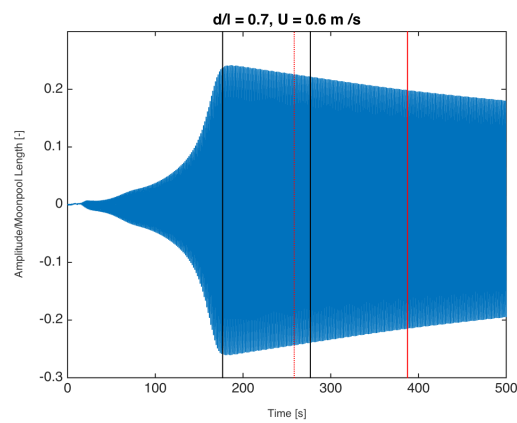
Figure B.1: Final results for a single case
Domain (0,0)(L,L) Mesh 60-90
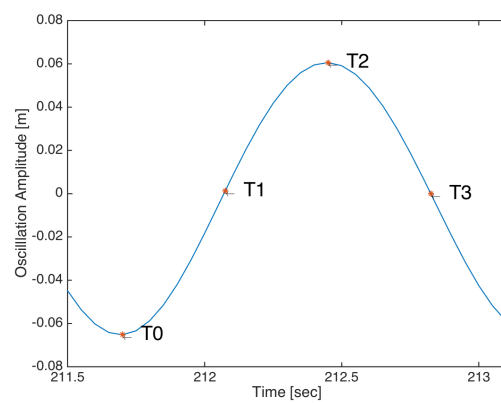
Figure B.2: Defintion of the sampled times.

(a) T0 - Vorticity

(b) T0 - Velocity

(c) T1 - Vorticity

(d) T1 - Velocity

(e) T2 - Vorticity

(f) T2 - Velocity

(g) T3 - Vorticity
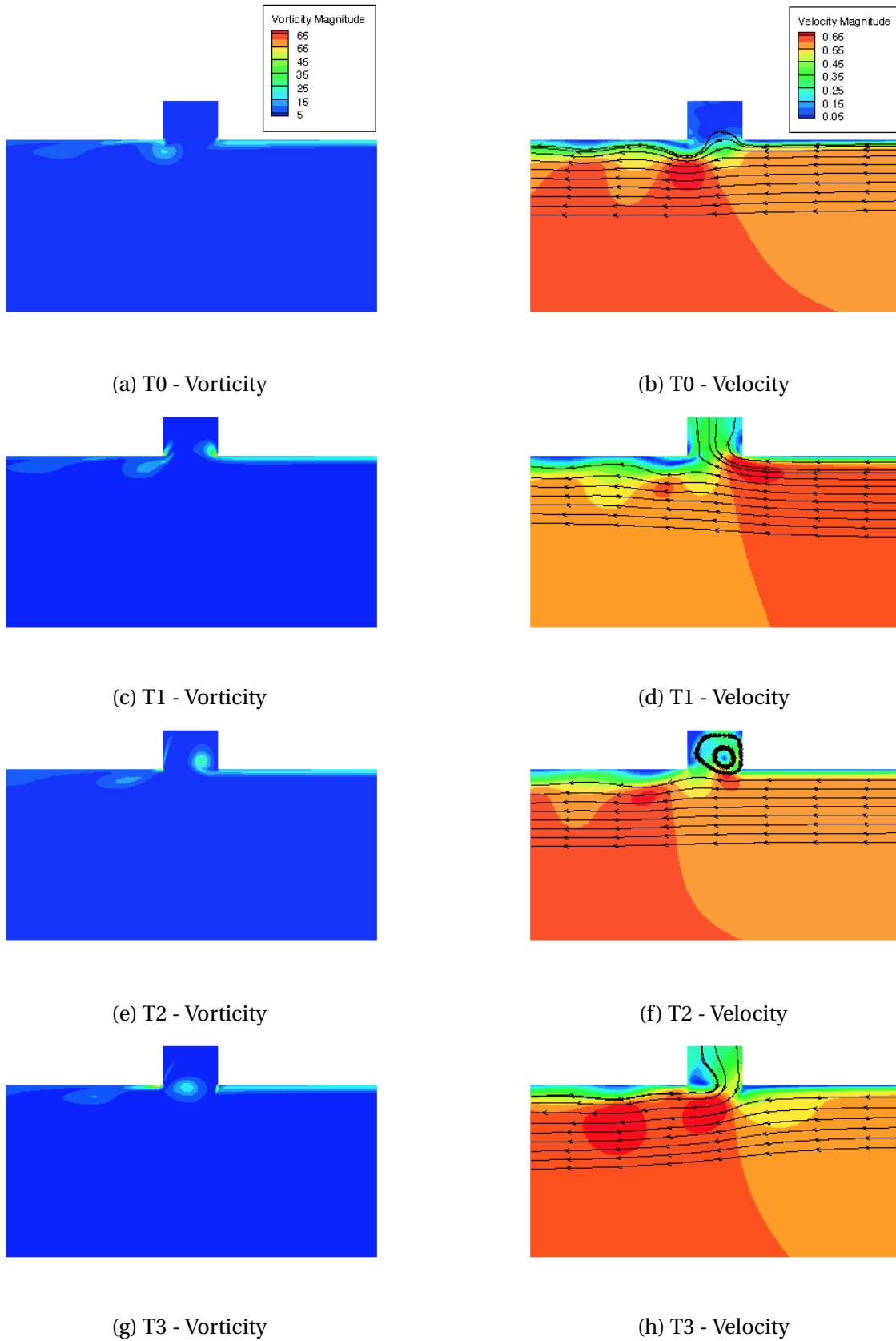
(h) T3 - Velocity

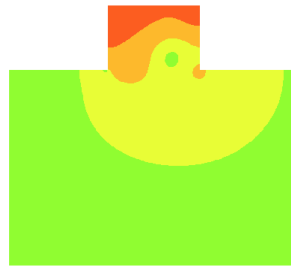Figure B.3: Vorticity and velocity magnitudes
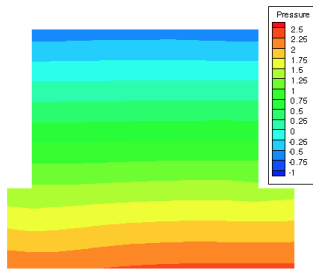
(a) T0 - Total Pressure
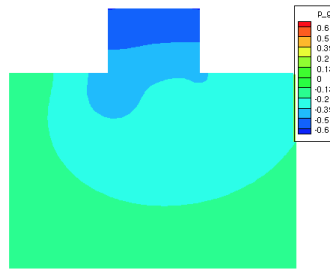
(b) T0 - Dynamic Pressure
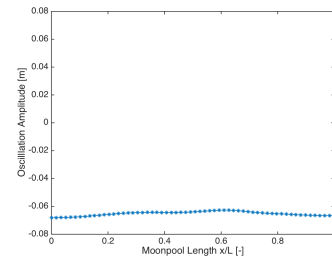
(c) T0 - Moonpool Amplitude
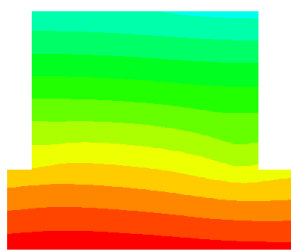
(d) T1 - Total Pressure

(e) T1 - Dynamic Pressure
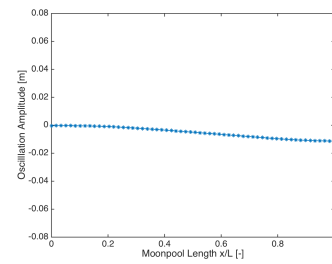
(f) T1 - Moonpool Amplitude
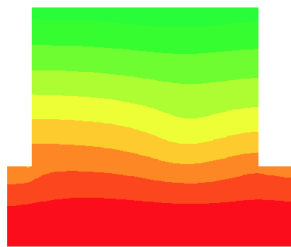
(g) T2 - Total Pressure

(h) T2 - Dynamic Pressure
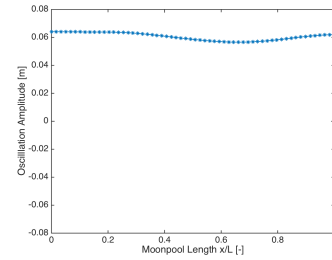
(i) T2 - Moonpool Amplitude
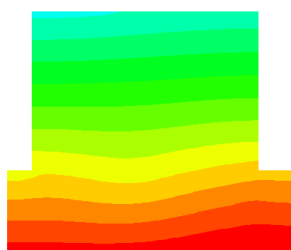
(j) T3 - Total Pressure
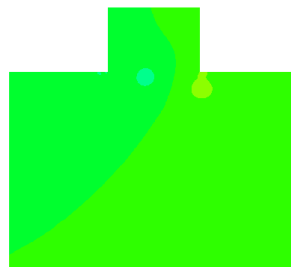
(k) T3 - Dynamic Pressure
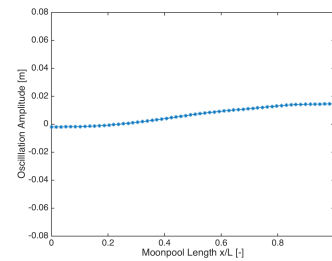
(l) T3 - Moonpool Amplitude

Figure B.4: Dynamic pressure and moonpool amplitude

No. 1 $t=0.04\,T$ ▶
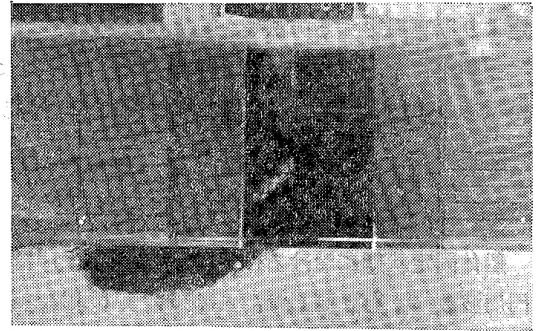
No. 2 $t=0.27\,T$ ▶
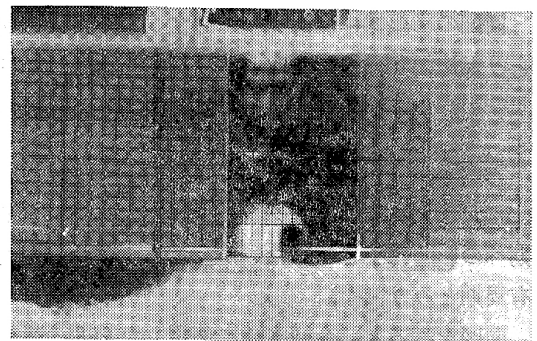
Condition	Ship is Fixed	
d = 0.12 m	U = 0.39 m/sec	$2U/\ell\omega_0 = 0.9$
ℓ/d = 1.0	T = 0.87 sec	Shutter Speed $^1/_{25}$ sec
b/d = 2.0	h = 11.4 mm	
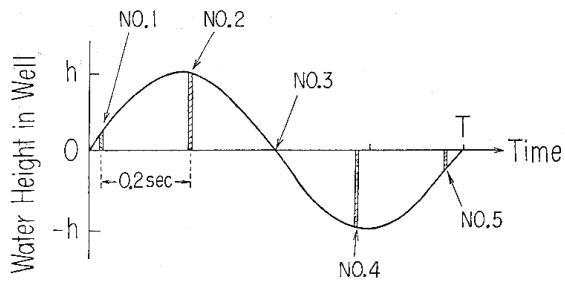
Fig. 5 Water Level in Well correspond with Photo. 1
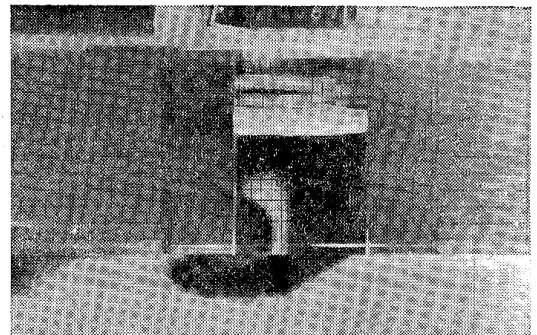
No. 3 $t=0.50\,T$ ▶
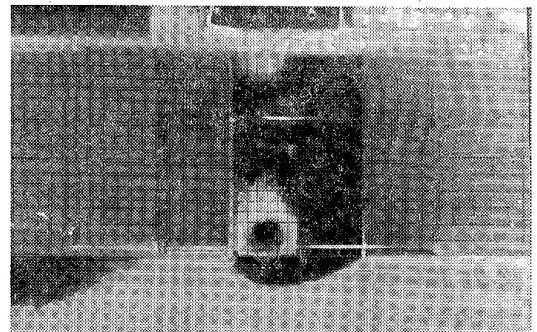
No. 4 $t=0.73\,T$ ▶

Figure B.5: Flow visualisation from Fukuda (1977).

Appendix C

Piston Mode Development

C.1 Moonpool draft-to-length 0,7

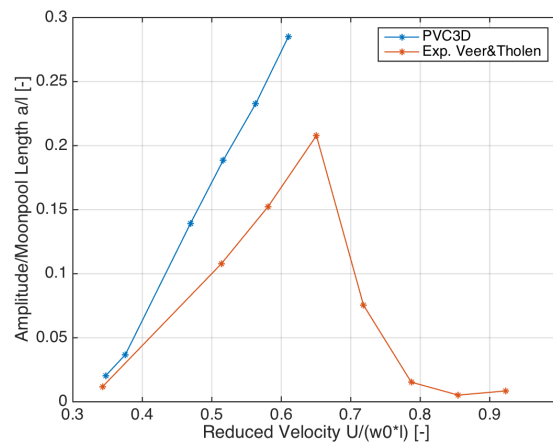| Velocity m/s^2	Reduced Velocity −	Non-Dimensional Amplitude −
0,37	0,357	0,0204
0,40	0,385	0,0368
0,50	0,482	0,1393
0,55	0,530	0,1885
0,60	0,578	0,2328
0,65	0,626	0,2850
0,75	0,675	0

Table C.1: Extracted results from Figure C.2

Figure C.1: Piston mode amplitude versus reduced velocity, d/l = 0.7
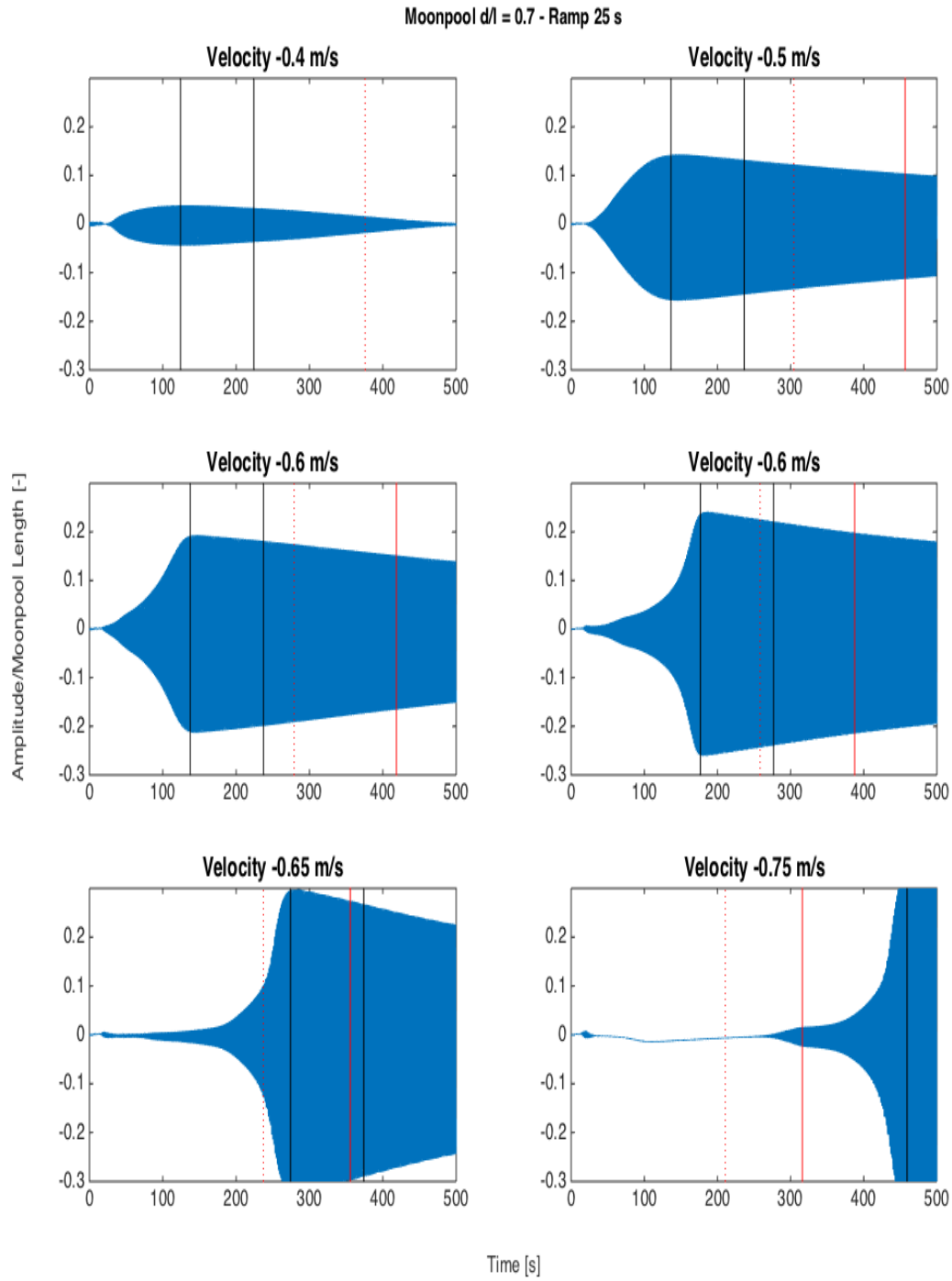
Figure C.2: Oscillations over time for different velocities, d/l = 0.7

C.2 Moonpool draft-to-length 0,6

Velocity m/s^2	Reduced Velocity –	Non-Dimensional Amplitude –
0,40	0,358	0,029
0,55	0,492	0,1656
0,65	0,582	0,2431
0,70	0,627	0,292
0,75	0,675	0

Table C.2: Extracted results from Figure C.4
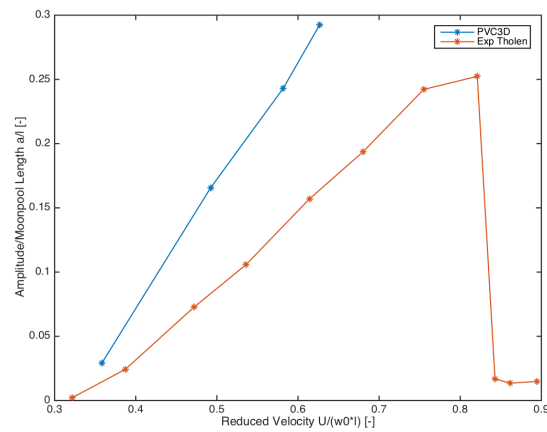
Figure C.3: Piston mode amplitude versus reduced velocity, d/l = 0.6
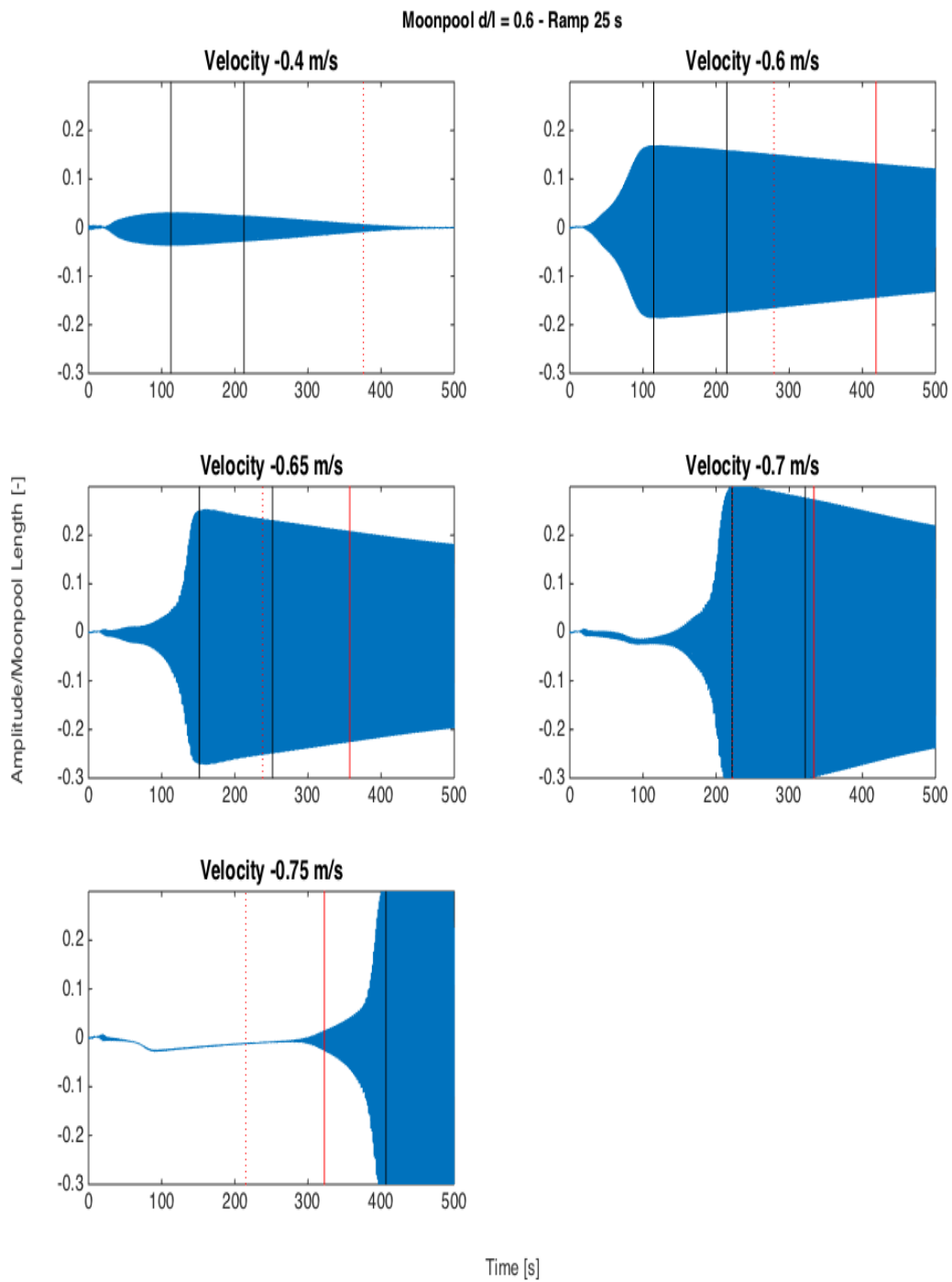
Figure C.4: Oscillations over time for different velocities, d/l = 0.6
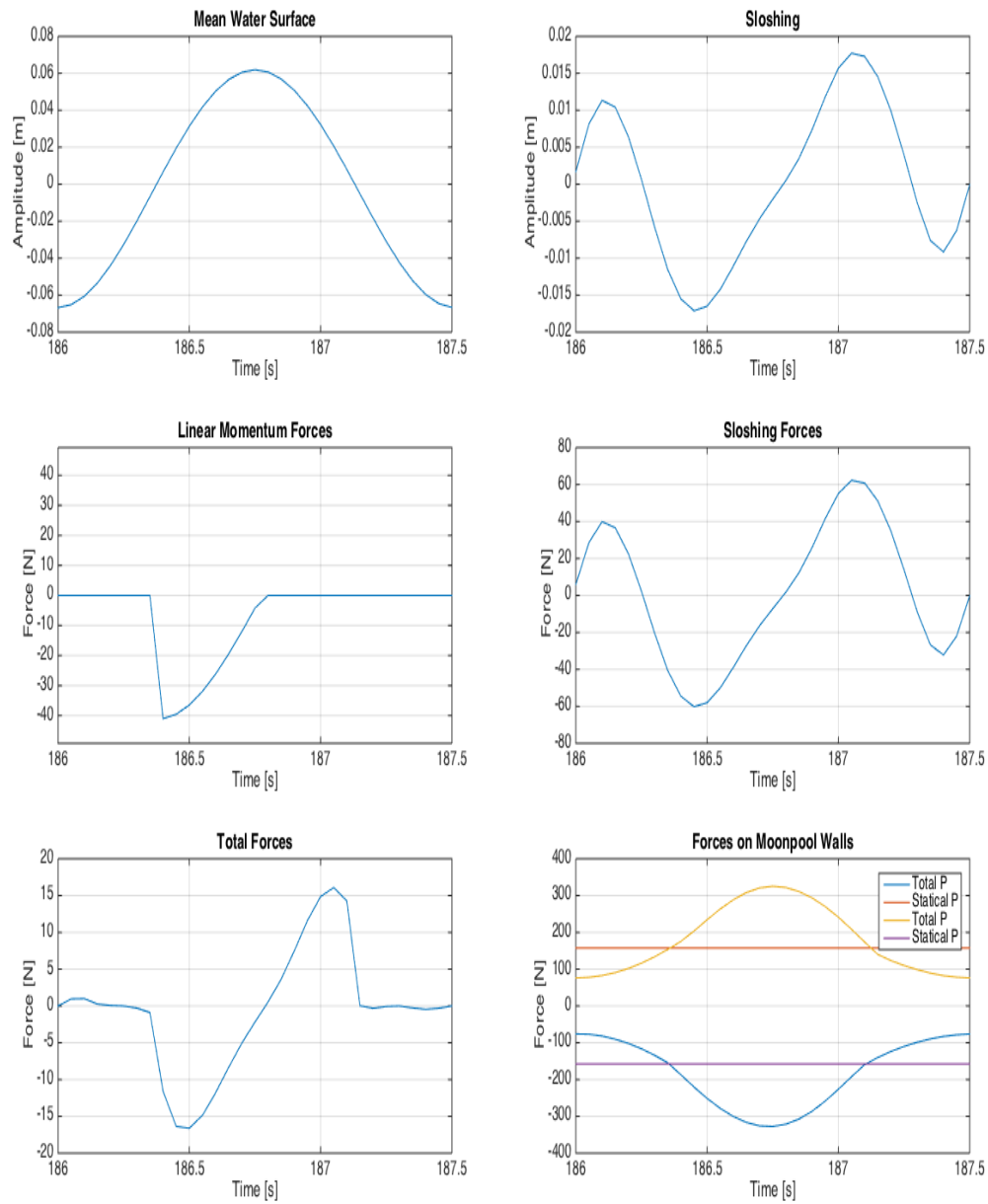
Appendix D

Forces On The Moonpool Walls

Figure D.1: Water elevations and 2D forces over a period

Appendix E

Moonpool Resistance Coefficient

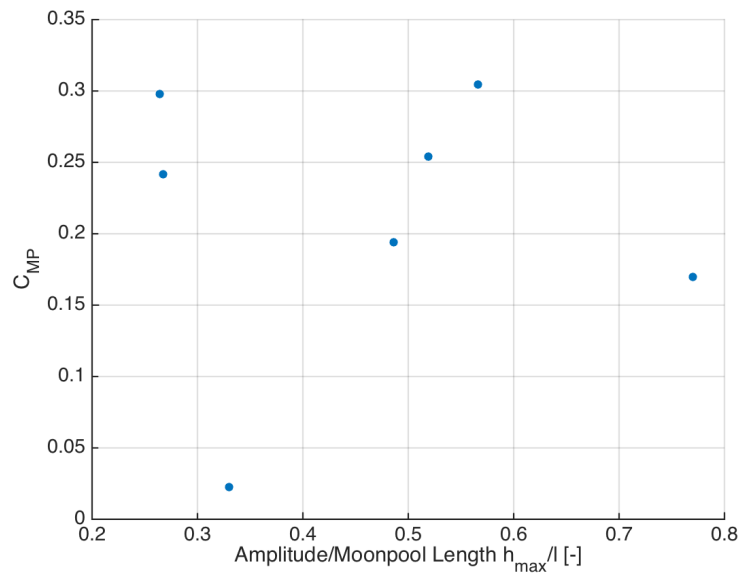Figure E.1: Moonpool resistance coefficient as a function of non-dimensional amplitude.

Appendix F

Digital Appendices

As this thesis is due to be delivered on the central computer system at the university, a number of files was digitally attached in the submission.

Poster.pdf
    A scientific poster was prepared for a display at the Tyholt Campus, Spring 2015.

OpenFOAM-towingTank.zip
    See note 1.

OpenFOAM-forcedHeave.zip
    See note 1.

Note 1: The two different cases as explained in the thesis are attached in two separate zip-files. Each folder contains a OpenFOAM-template and a MATLAB script that prepares the simulation campaigns. The campaigns can be run from a single *Allrun* command.

The templates assumes that OpenFOAM, PVC3D, GNU m4 and GNU Octave is installed.